GeoScienceWorld
Lithosphere
Volume 2023, Article ID 8019744, 38 pages
https://doi.org/10.2113/2023/8019744

Lithosphere

Research Article

Crust-Mantle Interaction Controls the Formation of High-Mg Adakitic Rocks: Evidence from Early Cretaceous Intrusive Complexes in Luxi Terrane, North China Craton

Songyan Liu,[1] Kangxing Shi,[1] Da Zhang,[1] Changming Wang,[1] Bin Du,[2] Qi Chen,[1] and Lei Gao[1]

[1]*School of Earth Sciences and Resources, China University of Geosciences, Beijing 100083, China*
[2]*Science and Technology Department, China Non-ferrous Metals Resource Geological Survey, Beijing 100012, China*

Correspondence should be addressed to Changming Wang; wangcm@cugb.edu.cn

Received 24 November 2022; Accepted 25 July 2023; Published 11 September 2023

Academic Editor: Jiyuan Yin

High-Mg adakite rocks preserve crucial information about the crust-mantle interactions during the magma evolution. The Luxi Terrane, southeastern North China Craton, stores a set of Early Cretaceous high-Mg adakite rocks; nevertheless, their petrogenesis remains controversial. In this study, we present new whole-rock geochemistry, zircon U-Pb-Hf isotopes in the Tiezhai, Jinxingtou, and Sanshanyu complexes which are composed of gabbroic diorite, diorites, syenites, and monzonites. Field observations and zircon U-Pb dating indicate that all of the rock units crystallized contemporaneously at ca. 125–120 Ma. They are characterized by high Al_2O_3 and Sr contents, and low MgO, Y, Yb, and heavy rare earth elements contents, coupled with high Sr/Y values (42–163), showing adakitic affinities. The magma mixing process is supported by the following ample evidence: (1) the disequilibrium mineral textures and mafic enclaves; (2) high $Mg^{\#}$ values (37–69, Mean = 58); and (3) widely zircons $\varepsilon_{Hf}(t)$ values (−25.6 to +7.8). The signature geochemical characteristics support that the adakites were generated by magma mixing of ancient crust-derived melts and relatively mafic melts from metasomatized mantle source. In combined with regional geology, the Early Cretaceous high-Mg adakites in Luxi Terrane represent the magmatic response of intensive crust-mantle interaction caused by the underplating of voluminous mantle-derived magma in an extension intracontinental setting.

1. Introduction

The traditional "Adakite" is referred to as intermediate-felsic magmatic rock associated with young and hot subduction and is characterized by high Sr/Y (>40) and La/Yb (>20) ratios, depletion in Nb and Ta and a lack of obvious Eu anomalies [1, 2]. In addition, some Mesozoic intracontinental high-Mg adakitic rocks (HMARs) with these geochemical signatures were detected in the North China Craton (NCC) [3–6]. HMAR are characterized by $Mg^{\#}$ > 50 (molar Mg/[Mg+Fe]) and high Ni, Cr, Sr, and Ba contents, low heavy rare earth element (HREE), which are hypothesized to have resulted from an interaction between the ascending felsic magmas and the mantle peridotite [4, 5]. However, if the high-Mg adakitic magmas observed in intracontinental environments are not primitive, their high-Mg adakitic signatures might be related to alternative processes including magma mixing and/or assimilation fractional crystallization (AFC) process [4, 7, 8]. These rocks and corresponding magmas can be termed as "High Sr/Y granitoids," and their geological implications are thus distinct from those based on assumptions that they are primitive magmas [6, 9–11]. Therefore, the petrogenetic mechanism of these HMAR needs to be further investigated, and thus, we call them "High Sr/Y granitoids" in this paper.

Situated at the Luxi Terrane, eastern of the NCC, is characterized by widespread distribution of the Early

Cretaceous adakite rocks and is considered a typical area to study the process of crust-mantle interaction [4, 6, 11–13]. However, the petrogenesis of the Early Cretaceous "High Sr/Y granitoids" in the Luxi Terrane remains controversial, resulting in the ambiguity of the geodynamic process and mechanism. Based on previous studies, the generation of the "High Sr/Y granitoids" rocks can be produced by four possible models as follows: (1) partial melting of the subducted oceanic crust and the magma assimilation with the lower crust material of NCC [6, 14]; (2) magma mixing coupled with AFC of the parental basaltic magma [4, 9, 15]; (3) partial melting of the mafic rocks from the thickened lower crust [11, 13, 14, 16]; (4) partial melting of the delaminated lower crust and subsequent interaction with mantle peridotite [8, 17–19]. The complicated process of crust-mantle resulted in the formation of multiple sources of adakite rocks. Therefore, we present new geological, petrological, whole-rock geochemical, zircon U-Pb, and Lu-Hf isotopic data from a suite of gabbroic diorite, diorite, and syenite in the Luxi Terrane, which were previously explained to be adakitic rocks and originated from partial melting of the enriched mantle and the magma assimilation with ancient crust [20].

Our objective is to provide particular constraint on crust-mantle interaction during the Early Cretaceous. The systematic petrological observation, zircon U-Pb-Hf isotopes, whole-rock geochemistry, and element modeling support that the adakitic samples were predominantly formed by the magma mixing of ancient crust-derived felsic melts and metasomatized mantle-derived mafic melts. The high-Mg adakitic porphyries in Jinxingtou, Tiezhai, and Sanshanyu Complexes stand for the magmatic products of intensive crust-mantle interaction induced by underplating of voluminous mantle-derived magma in an extension setting.

2. Geological Background

These "High Sr/Y" samples are located in the Luxi Terrane, as adjacent to the Tan-Lu fault (Figure 1(a)). In order to understand the geological context of the origin of these samples, we summarize some key information of the Luxi Terrane and the NCC as follows.

2.1. Regional Geology. The NCC is one of the world's oldest cratons [21–31] and has undergone significant lithospheric thinning and decratonization (or destruction) in the Mesozoic and Early Cenozoic eras [23, 32–35]. The thick and enriched lithospheric mantle was strongly weakened and gradually replaced by the thinner and depleted oceanic mantle in the Early Cretaceous, evidenced by the mantle xenoliths from the Paleozoic kimberlites and Cenozoic basalts [23, 35–38]. The NCC is located in the northeastern of China and composed of the eastern and western blocks amalgamated by the Trans-North China Orogen, which was also bounded by the Triassic Qinling-Dabie-Sulu Orogen in the south and the Late Paleozoic-early Mesozoic Central Asian Orogenic Belt in the north (Figure 1(b)) [21, 22, 27, 30, 31, 33, 39–41]. The NCC was cratonized at 1.85 Ga, and much of it had been stable up to the Triassic. However, the eastern part of the NCC had been reactivated since the early Mesozoic, as indicated by the occurrence of voluminous Mesozoic magmatic rocks and the formation of large-scale sedimentary basins. Most Mesozoic magmatic rocks in the NCC have intermediate to felsic compositions, with U-Pb zircon ages of 130–120 Ma, accompanied by small amounts of coeval mafic rocks [33]. The voluminous occurrence of Mesozoic HMARs in the eastern NCC has been generally considered to represent partial melts of the delaminated lowermost part of thickened continental crusts at great depths [4, 18, 42].

The present research focuses on the Luxi Terrane, which is a large uplifted region in the eastern blocks, separated by the Tan-Lu fault [21, 24, 28]. Precambrian metamorphic basement in the Luxi Terrane mainly contains supracrustal sequences and large volumes of Archean intrusive rocks (up to 90%), which commonly underwent greenschist to lower amphibolite facies metamorphism [30, 31, 41–44]. These rocks are unconformably overlain by the upper part of the Neoproterozoic Tumen Group, which is in turn unconformably overlain by Cambrian to Ordovician shale, sandstone and limestone, and Mesozoic to Cenozoic units in the Jiaolai Basin [24, 39, 40].

The extensive adakitic magmatism in the Luxi Terrane mainly occurred at 132–120 Ma, coincident with the large-scale magmatism in Luxi Terrane (134, 119 Ma; Figures 2(a) and 2(b)). By integrating the results obtained from the published data, the ages of Late Mesozoic igneous rocks in the Luxi Terrane can be divided into three groups: (1) quartz monzonites and porphyritic syenites emplaced in the Early Jurassic (185, 175 Ma); (2) mafic dykes emplaced in the Late Jurassic (144, 143 Ma); and (3) emplaced in 134–119 Ma, mainly composed of granodiorites, monzonite, diorites, and gabbroic diorites [5, 6, 11, 14, 20, 45–56]. The group (3) magma events corresponding to the voluminous adakites indicate the crust-mantle interaction reached culmination, and this process lasted until ca. 121 Ma when the enriched mantle was replaced by the asthenosphere mantle of the NCC [34].

2.2. Field Geology. Based on our field work, the diorite, syenite, and monzonite porphyry samples were collected from the Tiezhai, Jinxingtou, and Sanshanyu complexes (Figures 3(a) and 3(b)). The porphyries intruded into the Precambrian basement and Paleozoic sediments, which occurred as a dike in the field. The host rocks display coarse-grained textures and numerous mafic magmatic enclaves (MMEs) (Figures 4(a) and 4(b)).

The Tiezhai Complex, with a cover area of 40 km^2, is located in the southwest of Linqu County and intruded in an unconformity contact into the Precambrian basement and Neoarchean Tonalite-trondhjemite-granodiorite (TTG). The intrusion consists mainly of quartz diorite porphyry, minor monzonite, and syenite porphyry. The quartz monzonite porphyry (129.0 ± 1.7 Ma) was cut through by the quartz monzonite porphyry (125.0 ± 1.6 Ma) [56]. Laser-ablation inductively coupled plasma mass spectrometry (LA-ICP-MS) zircon

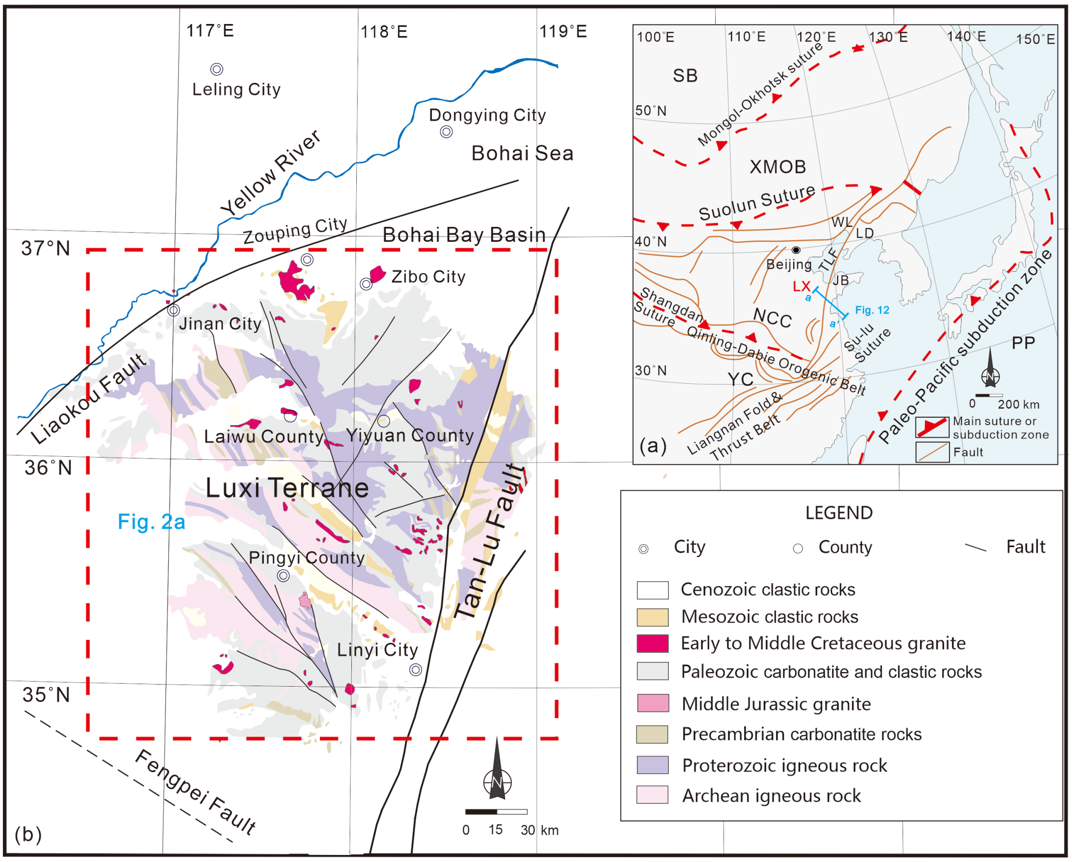

FIGURE 1: (a) Geological and tectonic framework of the NCC (modified from Reference 21). (b) Geological map of the Luxi Terrane (modified from Reference 92). Abbreviations: SB = Siberia Block, XMOB = Xing-Meng orogenic belt, NCC = North China Craton, YC = Yangtze Craton, PP = Pacific Plate, LX = Luxi Terrane, JB = Jiaobei Terrane, LD = Liaodong Peninsula, WL = Western Liaoning Province, and TLF = Tan-Lu Fault.

U-Pb ages show that this complex was emplaced at 125–129 Ma [14, 20, 47, 56, 57].

The Jinxingtou Complex, with an area of 11 km^2, is located in the central-eastern part of Luxi Terrane, southeast of Yiyuan County, intruded the unconformity between the Precambrian basement and Paleozoic limestone and shale. The intrusion mainly consists of diorite porphyry, gabbroic diorite, and syenite porphyry with Ar-Ar ages range from 120 to 121 Ma [58]. On the basis of previous studies, we provided new zircon U-Pb age and Lu-Hf isotope data and a new understanding of the petrogenesis of the intrusions.

The Sanshanyu Complex is located in the Sanshanyu village, 12 km^2 away from the Tiezhai Complex. This complex intruded the unconformity between the Precambrian basement and Paleozoic limestone and shale, consisting mainly of syenite and monzonite. These intrusive rocks carry MMEs in the syenite and monzonite. The age of the rocks from this complex has not been reported until now.

3. Methods

Whole-rock geochemistry analyses were conducted at the National Research Center for Geoanalysis, Beijing, China. Major elements and trace elements, including rare earth elements (REEs), were determined using standard X-ray fluorescence (XRF) and inductively coupled plasma mass spectrometry (ICP-MS) on a Finnigan MAT (Element I) instrument. The XRF analysis's accuracy is estimated to be better than 1% for SiO_2 and better than 2% for the other oxides. The ICP-MS analyses yield accuracies better than 5% for elements by multiple analyses of standards.

Zircon U-Pb geochronology was performed on an LA-ICP-MS at the State Key Laboratory of Continental Dynamics, Northwest University, Xi'an, China. Zircon U-Pb analysis was performed using a Neptune MC-ICP-MS equipped with a 193 nm excimer FX laser ablation system, with spot sizes of 32 μm. The 91,500 zircons with a weighted mean $^{206}Pb/^{238}U$ age of 1062.4 ± 5.9 Ma (2σ) and GJ-1 with a weighted mean age of 599.5 ± 4.0 Ma (2σ) were used as standards to monitor the ages of unknowns. Background subtraction and correction for laser-induced fractionation of U-Pb ratio signals were performed using Glitter 4.0. Concordia diagrams were constructed using Isoplot 4.15 [59].

In-situ zircon Hf isotopic analysis was analyzed at the State Key Laboratory of Geological Processes and Mineral Resources, China University of Geosciences, Wuhan, China. Zircon Hf isotopes were analyzed using a Neptune Plus

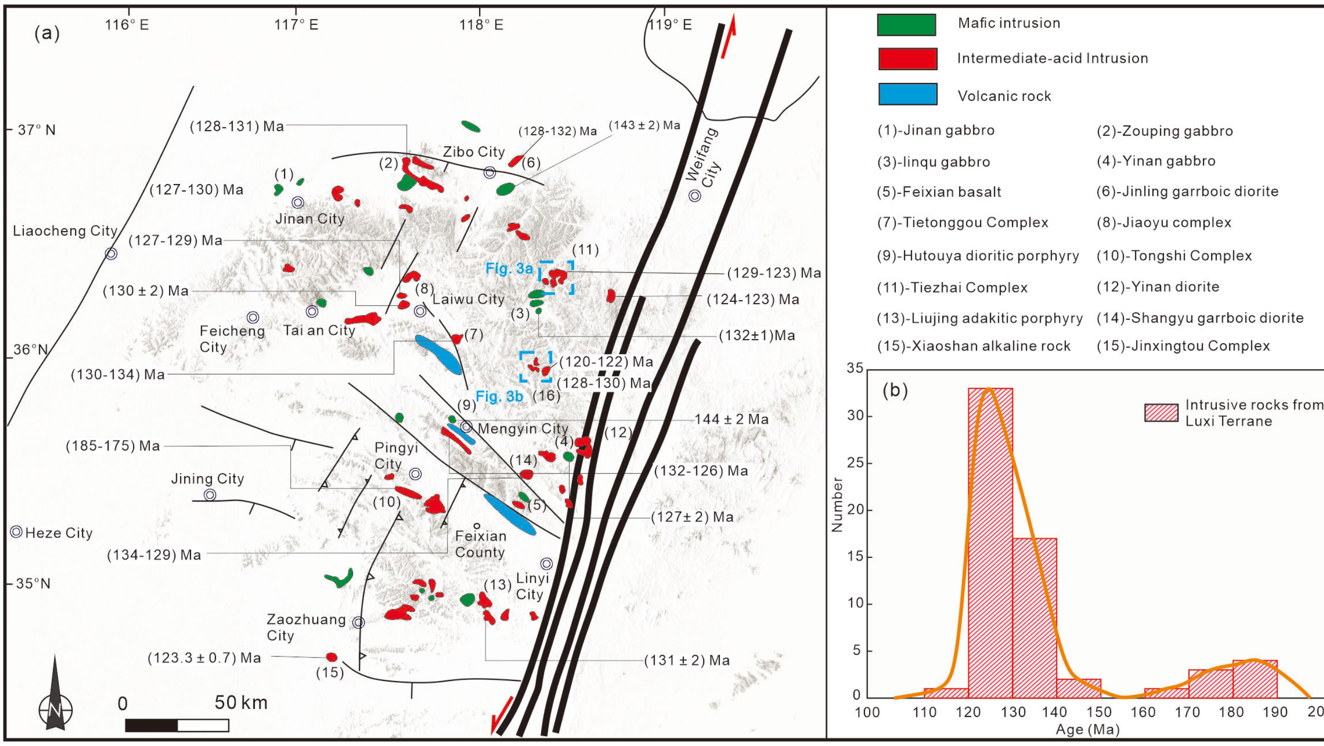

Figure 2: Spatial and temporal distribution map of the Mesozoic intrusive rocks in the Luxi Terrane (a, modified after Reference 93). (b) Histogram and probability curves of age from the Early Cretaceous intrusive rocks compiled from previous studies and this study in Luxi Terrane. Data sources: [3, 6, 11, 14, 17, 20, 45–53, 92, 94].

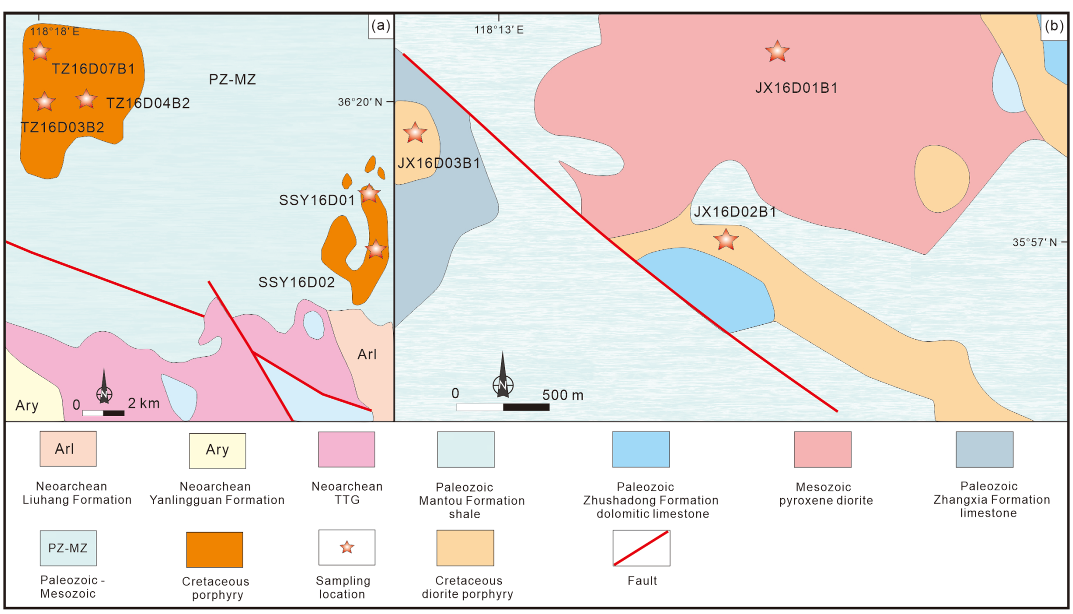

Figure 3: (a) Geological sketch map of the Tiezhai and Sanshanyu complexes (modified from Reference 20). (b) Geological sketch map of the Jinxingtou Complex (modified from Reference 58).

MC-ICP-MS in combination with a Geolas 2005 excimer ArF laser ablation system with spot sizes of 44 μm and a laser pulse frequency of 8–10 Hz. The initial $^{176}Hf/^{177}Hf$ value of 0.282785 and $^{176}Lu/^{177}Hf$ value of 0.0336 were calculated concerning the chondritic reservoir (CHUR) [60]. Depleted mantle model ages (T_{DM}) were calculated regarding the depleted mantle at the present $^{176}Hf/^{177}Hf$ value of 0.28325 and $^{176}Lu/^{177}Hf$ value of 0.0384 [61]. The Hf isotope crustal model ages (T_{DM}^{C}) were calculated by assuming that the samples' parental magma was derived from an average continental crust with a $^{176}Lu/^{177}Hf$ value of 0.015 and originated from a depleted mantle source [61].

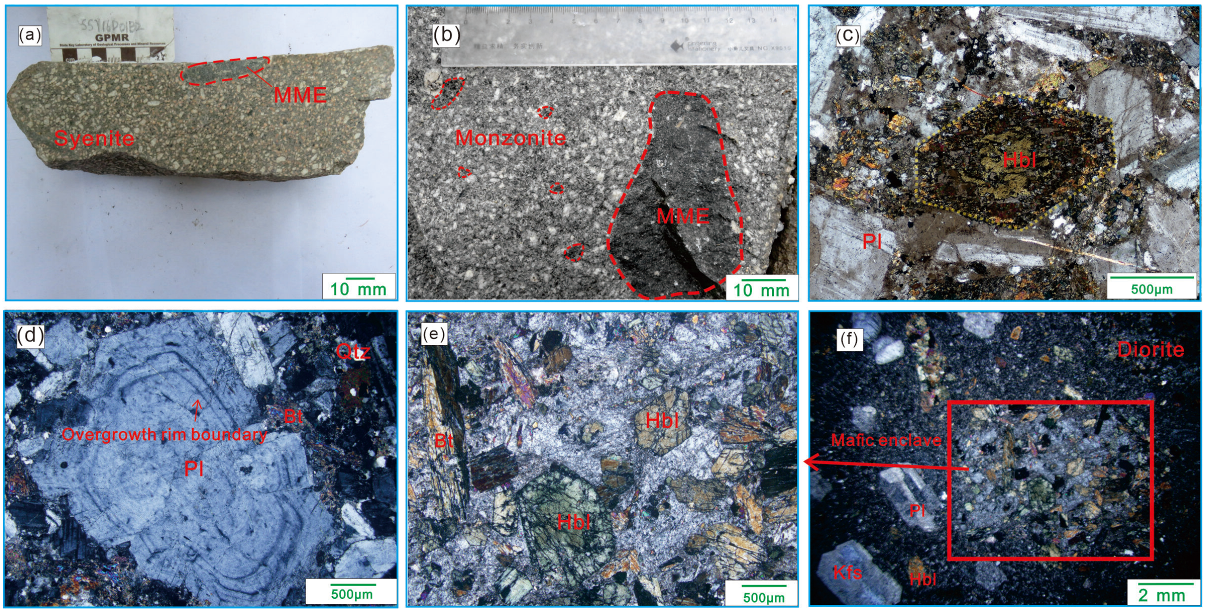

Figure 4: Representative photographs of hand specimens (a and b), and photomicrographs under cross-polarized light (c–f) showing the petrographic characteristics of the samples from the Luxi Terrane. (a and b) MME (mafic magmatic enclaves, marked by the red line) within porphyries and the sharp contact between them; (c) porphyritic syenite in which hornblende has well crystal shape; (d) Plagioclase showing obvious oscillatory zoning texture; (e and f) The hornblende gabbro is mingled enclaves enclosed in diorite host, and the pyroxene has been replaced by amphibole and biotite. Abbreviations: Bt = biotite; Hbl = hornblende; Pl = plagioclase; Qtz = quartz.

Off-line selection and integration of analyte signals were performed using ICP-MS Data Cal [62].

4. Results

4.1. Petrography. Three samples were collected from the Tiezhai Complex, 4 samples were collected from the Jinxingtou Complex, and 4 samples were collected from the Sanshanyu Complex (Table 1).

4.1.1. Tiezhai Complex. Two samples from the Tiezhai Complex are diorite with porphyritic texture. The diorites (Sample TZ16D03B2 and TZ16D04B2) were collected from the Yangtao and Maozihe village and are grayish green. They have a major mineral association of feldspar 55 vol.%, amphibole 25 vol.%, and quartz 3 vol.%, with accessory minerals of ilmenite, magnetite, zircon, and titanite <3% (Figure 5(a)). The plagioclase phenocrysts show grain sizes of 0.5–1.2 mm, and the matrix displays a fine-grained texture of 0.2–0.5 mm. The matrix consists of feldspar, quartz, and biotite 25 vol.%. The syenite Sample TZ16D07B1, collected from the Shanziyu village, is dark grayish and shows a medium-grained porphyritic texture. They have a major mineral association of feldspar 60 vol.%, amphibole 20 vol.%, quartz 3 vol.%, biotite <3%, and with zircon and magnetite as the accessory minerals. Feldspars are mainly composed of albite 1–5 mm, 30 vol.% and K-feldspar 0.5–5 mm, 30 vol.%. The matrix consists of feldspar and amphibole ~15 vol.%.

4.1.2. Jinxingtou Complex. The samples from the Jinxingtou Complex are gabbroic diorite and diorite with porphyritic texture. The gabbroic diorite (Sample JX16D01B1) was collected from the Majialing village and is grayish green. The pyroxene phenocrysts show grain sizes of 1–5 mm, and the matrix displays a fine-grained texture of 0.5–0.8 mm. They have a major mineral association of plagioclase 65 vol.% pyroxene 20%, amphibole 10 vol.%, quartz 3 vol.%, and zircon and magnetite <3% as the accessory mineral (Figure 5(a)).

The diorite Samples JX16D02B1, JX16D03B1, and JX16D03B3 that were collected from Xiyaozizhai and Maoziyu villages were green grayish with porphyritic texture. The enclaves enclosed in the diorite host are mainly composed of hornblende and plagioclase (Figures 4(e)–4(f)). The diorites are normally fine-grained at locations without mafic enclaves. The feldspar phenocrysts show grain sizes of 1–1.5 mm, and the matrix displays a fine-grained texture of 0.2–0.5 mm. They have a major mineral association of plagioclase 40 vol.%, amphibole 25 vol.%, quartz 3 vol.%, and zircon and magnetite <3% as the accessory minerals. The matrix consists of feldspar and amphibole ~30 vol.% (Figure 5(a)).

4.1.3. Sanshanyu Complex. The Sanshanyu complex is composed of syenite, monzogranite, and MMEs within them. Both the MMEs in the monzogranites and syenites are globular, ellipsoidal, or lenticular with heterogeneous orientation and lengths ranging from 5 cm to tens of centimeters and occasionally up to 30 cm. The syenites (Sample SSY16D01B1 and SSY16D01B2) are grayish yellow in color and show porphyritic texture. The albite and subordinate K-feldspar phenocrysts show grain sizes of 1–8 mm and 0.6–5.0 mm, respectively, and the matrix

Table 1: Rock types, locations, and mineralogy of samples from the Tiezhai, Jinxingtou, and Sanshanyu complexes in the Luxi Terrane.

No.	Samples	Rock types	Locality	GPS readings	Mineralogy
1	TZ16D03B2	Diorite porphyry	Yangtao village	N 36°20′36″; E 118°18′47″	Pl + Hbl + Qtz + Bt + Mt
2	TZ16D4B2	Diorite	Miaozihe village	N 36°20′22″; E 118°18′53″	Pl + Hbl + Qtz + Bt + Mt
3	TZ16D07B1	Monzonite porphyry	Shanziyu village	N 35°21′50″; E 118°18′05″	Kfs + Ab + Qtz + Hbl + Mt
4	JX16D01B1	Diabase porphyry	Majialing village	N 35°57′40″; E 118°14′04″	Px + Pl + Qtz + Mt
5	JX16D02B1	Diorite porphyry	Xiyaozhai village	N 35°57′24″; E 118°14′27″	Pl + Kfs + Qtz + Hbl + Mt
6	JX16D03B1	Diorite porphyry	Maoziyu village	N 35°57′49″; E 118°13′36″	Pl + Kfs + Qtz + Hbl + Mt
7	JX16D03B3	Diorite porphyry	Maoziyu village	N 35°57′47″; E 118°13′15″	Pl + Kfs + Qtz + Hbl + Mt
8	SSY16D01B1	Syenite porphyry	Sanshanyu village	N 36°17′17″; E 118°35′19″	Pl + Kfs + Qtz + Bt + Hbl + Mt
9	SSY16D01B2	Syenite porphyry	Sanshanyu village	N 36°17′17″; E 118°35′19″	Pl + Kfs + Qtz + Hbl + Mt
10	SSY16D02B1	Monzonite porphyry	Sanshanyu village	N 36°16′21″; E 118°35′34″	Pl + Qtz + Hbl + Mt
11	SSY16D02B3	Monzonite porphyry	Sanshanyu village	N 36°16′21″; E 118°35′34″	Pl + Qtz + Hbl + Mt

Qtz = quartz; Hbl = hornblende; Bt = biotite; Mt = magnetite; Kfs = K-feldspar; Pl = plagioclase

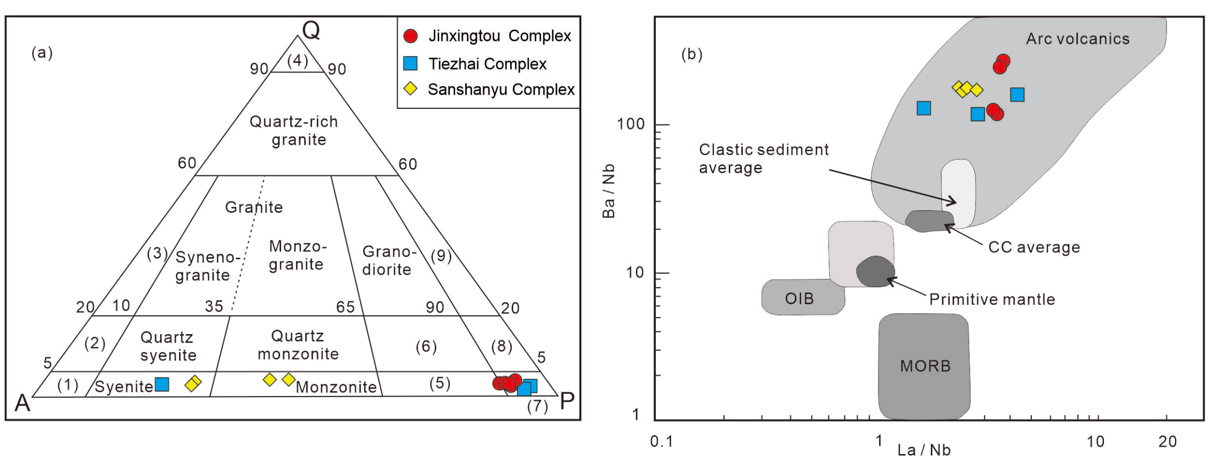

Figure 5: (a) Quartz-Alikali Plagioclase diagram [95]. (1) Alkali feldspar syenite; (2) quartz alkali feldspar syenite; (3) alkali feldspar granite; (4) quartzolite; (5) monzodiorite or monzogabbro; (6) quartz monzodiorite or quartz monzogabbro; (7) diorite, gabbro, or anorthosite; (8) quartz diorite, quartz gabbro, or quartz anorthosite; (9) trondhjemite. (b) Ba/Nb versus La/Nb plot showing that the "High Sr/Y granitoids" is characterized by high Ba/Nb and La/Nb ratios, falling in the field of arc volcanics. CC = continental crust and clastic sediment average [96]; MORB and OIB [97]; fields of arc volcanic rocks are from Reference 98.

displays a fine-grained texture of 0.1–0.5 mm. They have a major mineral association of albite 15 vol.%, K-feldspar 20 vol.%, amphibole 25 vol.%, quartz 3% vol.%, and zircon and magnetite <3% as the accessory minerals. The matrix consists of feldspar ~30 vol.% (Figure 5(a)).

The monzonites (Sample SSY16D02B1 and SSY16D02B3) are green grayish with a porphyritic texture. The plagioclase and K- feldspar phenocrysts show grain sizes of 0.5–5 mm and 0.1–5 mm, respectively, and the matrix displays a fine-grained texture of 0.2–0.5 mm. They have a major mineral association of plagioclase 25 vol.%, K-feldspar 20 vol.%, amphibole 20 vol.%, quartz <3 vol.%, and zircon and magnetite as the accessory minerals. The matrix consists of feldspar and quartz ~30 vol.% (Figure 5(a)).

4.2. Whole-Rock Geochemistry. The major and trace element compositions of eleven samples, including gabbroic diorite, diorite, monzonite, and syenite, are shown in Table 2.

The gabbroic diorite (Sample JX16D01B1) is characterized by low SiO_2 (52.1 wt%), high MgO (8.8 wt%), TFeO (9.4 wt%), Cr (420 ppm), and Ni (95 ppm) concentrations and $Mg^{\#}$ values (62). The rock is plotted in the gabbro fields in the total alkalis versus silica (TAS) diagram (Figure 6(a)) and belongs to the high-K calc-alkaline series (Figure 6(b)). It also shows enrichment in LREE ($[La/Yb]_N$ = 5.11) with no obvious Eu anomalies (δEu = 0.9) on chondrite-normalized REE patterns (Figure 6(e)). In the primitive mantle-normalized multielement diagram (Figure 6(f)), this sample exhibit negative Nb, Ta, and Ti anomalies and positive anomalies in large ion lithophile elements (LILEs; Ba, Rb, Pb, and K).

The diorite samples (Samples TZ16D03B2, TZ16D04B2, JX16D02B1, JX16D03B1, and JX16D03B3) are characterized by SiO_2 (57.6, 63.3 wt%), low MgO (2.75, 4.79 wt%), TFeO (3.9, 6.5 wt%), Cr (84, 211 ppm), and Ni (30.9, 50.7 ppm) concentrations and $Mg^{\#}$ values (55–69). The rocks are plotted in the diorite fields in the TAS diagram (Figure 6(a)), belong to the high-K calc-alkaline and calc-alkaline series (Figure 6(b)), and commonly plot in the peraluminous field (Figure 6(c)). On a chondrite-normalized REEs pattern, they are enriched in LREE ($[La/Yb]_N$ = 8.9–13.9) with no obvious Eu anomalies (δEu = 0.93–1.04; Figure 6(e)). In the primitive mantle-normalized multielement diagram (Figure 6(f)), they exhibit negative Nb, Ta, and Ti anomalies and positive anomalies in LILEs (Ba, Rb, Pb, and K).

The syenite samples (Samples TZ16D07B1, SSY16D01B1, and SSY16D01B2) are characterized by SiO_2 (64.2, 65.9 wt%), low MgO (0.7, 3.9 wt%), TFeO (2.2, 4.2 wt%), Cr (20.6, 218 ppm), and Ni (5.4, 61.3 ppm) concentrations and $Mg^{\#}$ values (37–62). The rocks are plotted in the syenite fields in the TAS diagram (Figure 6(a)), belong to the high-K calc-alkaline series (Figure 6(b)), and commonly plot in the peraluminous field (Figure 6(c)). Syenite samples are also LREE enriched ($[La/Yb]_N$ = 13.6–33.5) with no obvious Eu anomalies (δEu = 1.02–1.09, Figure 6(e)). In the primitive mantle-normalized multielement diagram (Figure 6(f)), they exhibit negative Nb, Ta, and Ti anomalies and positive anomalies in LILEs (Ba, Rb, Pb, and K).

The monzonite samples (Samples SSY16D02B1 and SSY16D02B3) are characterized by SiO_2 (61.9, 64.9 wt%), MgO (3.2, 4.3 wt%), TFeO (3.5, 4.3 wt%), Cr (184, 271 ppm), and Ni (53.0, 80.6 ppm) concentrations and $Mg^{\#}$ values (62–64). The rocks are plotted in the syenite fields in the TAS diagram (Figure 6(a)), belong to the high-K calc-alkaline series (Figure 6(b)), and are commonly plotted in the peraluminous field (Figure 6(c)). In the primitive mantle-normalized multielement diagram (Figure 6(e)), they exhibit negative Nb, Ta, and Ti anomalies and positive anomalies in LILEs (Ba, Rb, Pb, and K). They show LREE-enriched REEs patterns ($[La/Yb]_N$ =13.6–33.5) with no obvious Eu anomalies (δEu = 1.02–1.09, Figure 6(f)).

4.3. Zircon U-Pb Dating. LA-ICP-MS zircon U-Pb geochronology analysis was conducted on 8 samples from the Tiezhai, Sanshanyu, and Jinxingtou complexes (Figures 7(a)–7(h)). The zircon U-Pb dating results are listed in Table 3.

4.3.1. The Diorite (Sample TZ16D03B2, TZ16D04B2, JX16D02B1, and JX16D03B1). Zircons from the diorite porphyry sample (Sample TZ16D03B2) display magmatic oscillatory zoning without dark residual cores (Figure 7(a)). The grains are colorless or dark brownish, with a maximum length of 100 μm and a length-to-width ratio of 1.5:1 to 1:1. The zircon grains show an extensive range of Th (7, 2341 ppm) and U (9, 1164 ppm) contents, with Th/U ratios varying from 0.05 to 2.3. Fifteen concordant spots yield a weighted mean $^{206}Pb/^{238}U$ age of 125 ± 1 Ma (MSWD = 0.33), and three xenocrystic grains yield $^{207}Pb/^{206}Pb$ ages of 2513, 2354, and 2512 Ma.

Zircon grains from the diorite sample (Sample TZ16D04B2) show magmatic oscillatory zoning, with a maximum length of 150 μm and a length-to-width ratio of 2:1 to 1:1 (Figure 7(b)). Fifteen analyzed spots have Th contents in the range of 149–1149 ppm, U contents in the range of 147–1937 ppm, and Th/U values of 0.3–1.79. They yield a weighted mean $^{206}Pb/^{238}U$ age of 123 ± 1 Ma (MSWD = 1.6).

Sixteen zircon grains from the diorite porphyry sample (sample JX1602B1) were obtained for zircon U-Pb geochronology (Figure 7(d)). The grains are colorless or dark brownish, with a clear core-rim structure and a maximum length of 150 μm and a length-to-width ratio of 1.5:1 to 1:1. Twenty spots show 78–446 ppm Th and 8–828 ppm U with Th/U values of 0.2–1.4. Ten spots yield a weighted mean $^{206}Pb/^{238}U$ age of 120 ± 1 Ma (MSWD = 1.3). Ten other spots define a weighted mean $^{207}Pb/^{206}Pb$ age of 2529 ± 6 Ma.

Zircon grains from the diorite porphyry sample (sample JX16D03B1) show a large range of Th (31, 696 ppm) and U (74, 949 ppm) contents, with Th/U ratios varying from 0.1 to 6.3 (Figure 7(e)). Based on 17 concordant spots, a weighted mean $^{206}Pb/^{238}U$ age of 122 ± 1 Ma (MSWD = 0.82) is obtained. Three xenocrystic grains yielded $^{207}Pb/^{206}Pb$ ages of 2551, 2505, and 2493 Ma (spot 1, 4, and 18).

4.3.2. The Syenite Samples (Samples TZ16D07B1, SSY16D01B1, and SSY16D01B2). The zircon grains from the syenite porphyry sample (Sample TZ16D07B1) were obtained for zircon U-Pb geochronology (Figure 7(c)). Seventeen grains are colorless or dark brownish, with a clear core-rim structure and a maximum length of 200 μm and a length-to-width ratio of 2:1 to 1:1. Seventeen analyzed spots have Th contents in the range of 73–346 ppm, U contents in the range of 371–818 ppm, and Th/U values of 0.07–0.67. Seventeen concordant data points form a tight cluster with a weighted mean $^{206}Pb/^{238}U$ age of 123 ± 1 Ma (MSWD = 1.4).

Table 2: Major (wt. %) and trace elements (ppm) geochemistry of samples from the Tiezhai, Jinxingtou, and Sanshanyu complexes in the Luxi Terrane.

Samples	TZ16D03 B2	TZ16D04 B2	TZ16D07 B1	JX16D01 B1	JX16D02 B1	JX16D03 B1	JX16D03 B3	SSY16D01 B1	SSY16D01 B2	SSY16D02 B1	SSY16D02 B3
Rock types	Diorite porphyry	Diorite	Monzonite porphyry	Diabase Porphyry	Diorite porphyry	Diorite porphyry	Diorite porphyry	Syenite porphyry	Syenite porphyry	Diorite porphyry	Diorite porphyry
SiO_2	57.6	57.8	62.9	49.1	60.	63.3	62.	61.	63.	60.8	63.9
TiO_2	0.7	0.6	0.2	0.9	0.6	0.4	0.4	0.4	0.4	0.5	0.4
Al_2O_3	15.8	15.9	16.8	13.8	15.7	15.9	15.9	15.1	15.6	15.9	15.6
FeO^T	3.90	6.42	2.11	8.93	5.09	3.99	3.96	4.01	3.55	4.24	3.50
Fe_2O_3	1.83	3.48	1.24	4.79	3.05	2.30	2.39	1.77	1.57	1.98	1.39
FeO	2.25	3.29	0.99	4.62	2.35	1.92	1.81	2.42	2.14	2.46	2.25
MnO	0.08	0.10	0.04	0.13	0.10	0.06	0.07	0.07	0.07	0.07	0.05
MgO	4.79	4.37	0.69	8.25	3.72	2.75	2.75	3.74	2.97	4.24	3.18
CaO	6.87	5.90	3.19	8.22	3.84	3.11	3.58	2.94	3.28	4.80	3.88
Na_2O	5.46	4.22	5.69	2.98	5.70	4.90	5.10	4.55	5.03	4.62	4.62
K_2O	2.59	2.53	3.45	1.35	1.81	2.99	2.42	3.19	2.81	2.66	3.07
P_2O_5	0.27	0.24	0.07	0.14	0.18	0.14	0.14	0.13	0.11	0.15	0.12
LOI	1.05	0.50	3.90	5.33	2.27	2.09	2.30	2.78	1.86	0.64	0.69
Total	99.59	99.35	99.43	100.10	99.68	100.14	99.62	99.13	99.23	99.11	99.37
A/CNK	0.65	0.78	0.89	0.65	0.86	0.94	0.90	0.93	0.90	0.83	0.87
Li	23.5	13.9	32.0	44.4	31.8	24.7	23.6	40.4	39.5	20.8	22.5
Be	1.73	1.55	2.86	1.02	1.66	1.74	1.84	2.36	2.63	2.31	2.48
Sc	16.7	17.0	3.03	34.3	14.8	9.61	10.0	10.5	9.34	11.3	9.87
V	162	137	25.4	246	152	80.4	82.5	83.2	71.6	89.0	76.7
Cr	211	139	20.6	420	84.0	90.9	91.6	218.0	163	271	184
Co	17.3	24.3	3.8	45.0	19.7	14.4	15.4	18.2	14.6	19.7	16.1
Ni	50.7	45.4	5.42	95.4	32.7	30.9	34.5	61.3	45.4	80.6	53.0
Cu	29.0	47.8	4.94	99.6	95.0	9.31	11.2	4.75	37.4	7.18	22.6
Zn	41.4	76.2	83.0	79.2	79.2	37.3	41.4	57.3	73.5	76.5	46.4
Ga	21.4	21.5	31.5	17.2	22.4	21.0	22.1	23.9	25.3	25.1	25.5
Rb	52.6	56.9	91.9	34.2	40.5	61.5	53.6	100	66.2	61.6	91.5
Sr	710	713	480	564	547	864	646	844	978	1107	973
Zr	158	113	236	64.3	111	99.2	104	106	108	143	109
Nb	6.90	5.54	9.90	3.67	5.29	4.68	4.81	6.42	6.30	6.40	6.67

(*Continued*)

Table 2: Continued

Samples	TZ16D03 B2	TZ16D04 B2	TZ16D07 B1	JX16D01 B1	JX16D02 B1	JX16D03 B1	JX16D03 B3	SSY16D01 B1	SSY16D01 B2	SSY16D02 B1	SSY16D02 B3
Rock types	Diorite porphyry	Diorite	Monzonite porphyry	Diabase Porphyry	Diorite porphyry	Diorite porphyry	Diorite porphyry	Syenite porphyry	Syenite porphyry	Diorite porphyry	Diorite porphyry
Mo	0.85	2.77	0.25	0.27	0.49	0.26	0.96	0.27	0.21	0.67	0.25
Cd	<0.05	0.12	<0.05	<0.05	0.07	<0.05	<0.05	0.13	0.07	0.09	0.05
In	<0.05	<0.05	<0.05	0.06	<0.05	<0.05	<0.05	<0.05	<0.05	<0.05	<0.05
Sb	0.20	0.09	0.23	0.33	0.35	0.25	0.68	0.51	0.32	0.07	0.06
Cs	1.55	2.55	4.82	1.30	1.53	2.20	1.64	2.24	2.87	2.97	1.40
Ba	817	892	1282	445	634	1275	1191	1167	1134	1159	1158
Hf	3.92	3.44	6.03	2.18	3.53	3.27	3.35	3.72	3.81	3.92	3.84
Ta	0.43	0.30	0.35	0.25	0.32	0.30	0.30	0.42	0.37	0.35	0.38
W	0.97	0.79	0.35	0.42	0.56	0.36	0.58	0.47	0.54	0.59	0.91
Tl	0.40	0.30	0.69	0.24	0.31	0.54	0.43	0.79	0.55	0.44	0.53
Pb	6.63	13.1	18.9	5.85	19.2	13.0	14.9	16.4	26.2	17.5	14.6
Bi	<0.05	<0.05	<0.08	<0.05	<0.05	0.40	0.52	0.08	0.07	<0.05	<0.05
Th	5.27	6.17	5.16	3.15	3.99	3.89	3.93	4.15	4.37	3.11	4.58
U	1.21	1.71	2.20	0.75	1.43	1.48	1.38	1.72	1.60	1.41	1.62
Y	12.4	11.8	3.38	13.3	9.03	6.98	7.35	6.72	6.00	7.31	6.52
La	19.5	23.6	15.9	12.4	18.2	17.2	17.1	15.7	14.6	16.1	18.6
Ce	41.7	47.1	31.2	26.2	36.7	33.1	32.8	30.4	28.6	33.1	36.8
Pr	5.69	6.19	3.86	3.71	4.83	4.16	4.20	4.00	3.72	4.48	4.62
Nd	25.4	26.7	15.9	17.3	21.5	17.2	17.6	17.7	15.9	19.9	19.3
Sm	4.53	4.53	2.63	3.65	3.74	2.98	2.97	3.20	2.90	3.68	3.38
Eu	1.33	1.34	0.80	1.09	1.09	0.96	0.96	1.00	0.98	1.16	1.08
Gd	4.12	4.17	2.02	3.68	3.29	2.52	2.58	2.67	2.46	3.01	2.79
Tb	0.54	0.53	0.21	0.52	0.42	0.32	0.31	0.32	0.30	0.37	0.32
Dy	3.02	2.89	0.90	3.17	2.31	1.75	1.74	1.72	1.56	1.87	1.67
Ho	0.58	0.55	0.14	0.64	0.43	0.32	0.34	0.31	0.28	0.35	0.31
Er	1.62	1.54	0.36	1.82	1.21	0.91	0.92	0.85	0.78	0.97	0.84
Tm	0.23	0.22	0.05	0.26	0.17	0.13	0.13	0.13	0.11	0.14	0.12
Yb	1.56	1.55	0.34	1.74	1.14	0.91	0.91	0.81	0.77	0.90	0.82
Lu	0.24	0.23	<0.05	0.26	0.17	0.14	0.14	0.13	0.11	0.13	0.12

(*Continued*)

Table 2: Continued

Samples	TZ16D03 B2	TZ16D04 B2	TZ16D07 B1	JX16D01 B1	JX16D02 B1	JX16D03 B1	JX16D03 B3	SSY16D01 B1	SSY16D01 B2	SSY16D02 B1	SSY16D02 B3
Rock types	Diorite porphyry	Diorite	Monzonite porphyry	Diabase Porphyry	Diorite porphyry	Diorite porphyry	Diorite porphyry	Syenite porphyry	Syenite porphyry	Diorite porphyry	Diorite porphyry
ΣREE	110	121	74.3	76.4	95.2	82.6	82.7	78.9	73.1	86.2	90.8
LREE	98.1	109	70.3	64.3	86.1	75.6	75.6	72.0	66.7	78.4	83.7
HREE	11.9	11.7	4.02	12.09	9.14	7.00	7.07	6.94	6.37	7.74	6.99
LREE/HREE	8.24	9.37	17.5	5.32	9.42	10.8	10.7	10.4	10.5	10.1	12.0
La_N/Yb_N	8.97	10.92	33.54	5.11	11.45	13.56	13.48	13.90	13.60	12.83	16.27
δEu	0.92	0.93	1.02	0.90	0.93	1.04	1.04	1.02	1.09	1.03	1.04
δCe	0.96	0.93	0.95	0.94	0.94	0.93	0.92	0.92	0.93	0.94	0.95

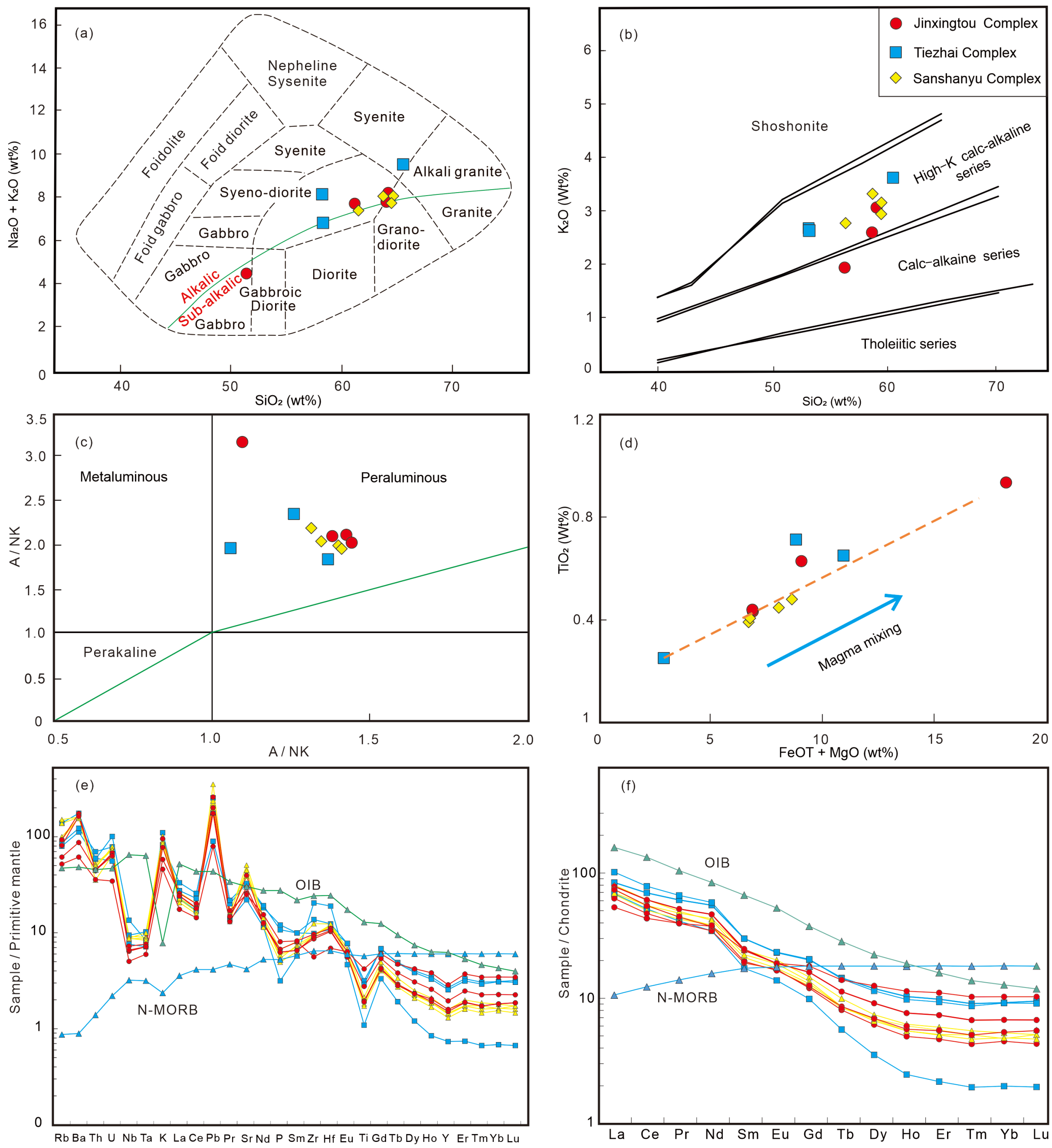

FIGURE 6: Geochemical signatures of "High Sr/Y granitoids" in the Luxi Terrane. (a) TAS diagram [97]; (b) K_2O versus SiO_2 diagram [99]; (c) A/CNK versus SiO_2 diagram. (d) Plot of TiO_2 versus FeOT + MgO. (e) Chondrite-normalized rare earth elements patterns [64]. (f) Primitive mantle-normalized spider diagrams [100].

The zircon grains from the syenite porphyry sample (sample SSYD01B1) display magmatic oscillatory zoning without dark residual cores (Figure 7(f)). The zircon grains show an extensive range of Th (42, 350 ppm) and U (345, 914 ppm) contents, with Th/U ratios varying from 0.2 to 0.4. Twenty spots yield a weighted mean age $^{206}Pb/^{238}U$ age of 124 ± 1 Ma (MSWD = 0.93).

Zircons from the syenite porphyry sample (Sample SSYD01B2) are brown and range in size up to 100 × 200 μm with a length-to-width ratio of around 2:1 (Figure 7(g)). They are generally euhedral to subhedral, and some grains have cloudy or patchy zoning. Twenty analyzed spots have Th contents in the range of 80–255 ppm, U contents in the range of 342–904 ppm, and Th/U values of 0.15–0.5. Twenty concordant spots yield a weighted mean $^{206}Pb/^{238}U$ age of 123 ± 1 Ma (MSWD = 1.7).

4.3.3. The Monzonite Sample (Sample SSY16D02B1). Zircons from the monzonite sample (Sample SSY16D02B1) are mostly brownish and range in size of 100 × 200 μm with a length-to-width ratio of around 2:1 (Figure 7(h)). They show euhedral to subhedral morphology, and some grains display patchy or

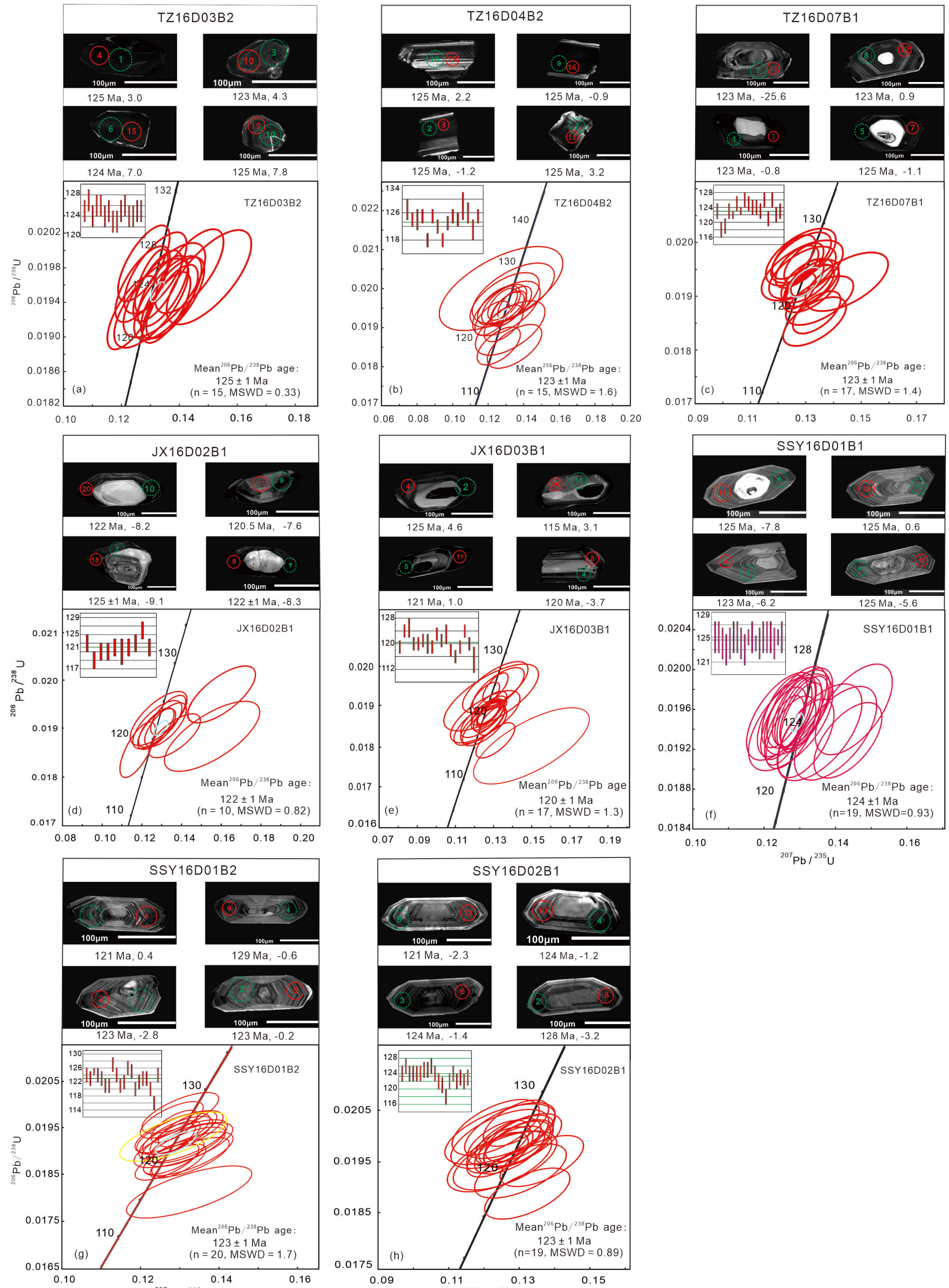

Figure 7: Cathodoluminescence images of representative zircons and zircon U-Pb concordia plots. The samples from the Tiezhai Complex: (a) TZ16D03B2, (b) TZ16D04B2, and (c)TZ16D07B1; the samples from the Jinxingtou Complex: (d) JX16D02B1 and (e) JX16D03B1; the samples from the Sanshanyu Complex: (f) SSY16D01B1; (g) SSY16D01B2; (h) SSY16D02B1. The larger green circle represents the spot of Lu-Hf analysis, and the smaller red circle represents the spot of U-Pb analysis. Spot number, U-Pb age in Ma, and the $\varepsilon_{Hf}(t)$ values are shown below of the zircons.

clouded zoning. Twenty analyzed spots have Th contents in the range of 61–259 ppm, U contents in the range of 398–806 ppm, and Th/U values of 0.1–0.4. Eleven concordant spots yield a weighted mean $^{206}Pb/^{238}U$ age of 123 ± 1 Ma (MSWD = 0.89).

Table 3: LA–ICP–MS zircon U-Pb data of samples from the Tiezhai, Jinxingtou, and Sanshanyu complexes in the Luxi Terrane.

	(ppm)			Isotopic ratios						Ages (Ma)					
Spots	Th	U	Th/U	$^{207}Pb/^{206}Pb$	±1σ	$^{207}Pb/^{235}U$	±1σ	$^{206}Pb/^{238}U$	±1σ	$^{207}Pb/^{206}Pb$	±1σ	$^{207}Pb/^{235}U$	±1σ	$^{206}Pb/^{238}U$	±1σ
TZ1603B2															
1	608.8	602.5	1.01	0.11754	0.00384	0.64511	0.01726	0.0398	0.00055	1919	29	505	11	252	3
2	1722	947.4	1.82	0.04709	0.00248	0.12733	0.00621	0.01961	0.00029	54	79	122	6	125	2
3	2341	1165	2.01	0.04667	0.00233	0.12775	0.00588	0.01985	0.00029	32	71	122	5	127	2
4	1290	679.9	1.90	0.05072	0.00306	0.13604	0.00769	0.01945	0.00032	228	100	130	7	124	2
5	1463	776.2	1.88	0.0484	0.00279	0.13173	0.0071	0.01974	0.00031	119	92	126	6	126	2
6	1.75	7.07	0.25	0.16551	0.0106	10.3043	0.66413	0.45145	0.01725	2513	59	2462	60	2402	77
7	855.9	464.1	1.84	0.05533	0.00376	0.15021	0.00965	0.01969	0.00036	426	111	142	9	126	2
8	3144	1199	2.62	0.05136	0.00241	0.1375	0.00588	0.01941	0.00028	257	72	131	5	124	2
9	1745	843.6	2.07	0.04812	0.00164	0.1304	0.00375	0.01965	0.00024	105	45	124	3	125	2
10	1141	954.6	1.20	0.05083	0.00227	0.13554	0.00548	0.01934	0.00027	233	67	129	5	123	2
11	1962	997.7	1.97	0.04655	0.00232	0.12376	0.00567	0.01928	0.00028	26	71	118	5	123	2
12	136.2	337.3	0.40	0.15074	0.00382	3.91747	0.08562	0.18848	0.00242	2354	44	1617	18	1113	13
13	575.5	394.3	1.46	0.05004	0.00364	0.13485	0.00933	0.01954	0.00036	197	123	128	8	125	2
14	929.6	621.1	1.50	0.05266	0.00305	0.14348	0.00777	0.01976	0.00032	314	94	136	7	126	2
15	1182	642.7	1.84	0.04873	0.00334	0.13033	0.00846	0.01939	0.00034	135	113	124	8	124	2
16	1555	670.4	2.32	0.05133	0.00289	0.13769	0.00722	0.01945	0.00031	256	91	131	6	124	2
17	7.37	146.7	0.05	0.1654	0.00384	10.3055	0.16195	0.45179	0.00561	2512	12	2463	15	2403	25
18	94.72	623.9	0.15	0.05105	0.00174	0.27567	0.00795	0.03915	0.00048	243	44	247	6	248	3
19	998.6	595.8	1.68	0.04987	0.00232	0.13431	0.00568	0.01953	0.00027	189	73	128	5	125	2
20	2071	942	2.20	0.04904	0.00225	0.13245	0.00552	0.01959	0.00027	150	71	126	5	125	2
TZ1604B2															
1	685.1	436.2	1.57	0.05317	0.02363	0.15504	0.06873	0.02115	0.00065	336	814	146	60	135	4
2	123.8	158.2	0.78	0.04892	0.00571	0.13414	0.01522	0.01988	0.00051	144	206	128	14	127	3
3	824.2	572	1.44	0.04869	0.00252	0.13077	0.00627	0.01947	0.00029	133	82	125	6	124	2
4	286.1	217.4	1.32	0.04848	0.00482	0.13027	0.01252	0.01949	0.00046	123	170	124	11	124	3
5	558.9	358.7	1.56	0.06276	0.00356	0.17572	0.00928	0.0203	0.00035	700	83	164	8	130	2
6	1135	584.7	1.94	0.04741	0.00222	0.12812	0.00549	0.0196	0.00027	70	70	122	5	125	2
7	341.1	282.8	1.21	0.09382	0.00309	0.61827	0.01694	0.04779	0.00064	1504	32	489	11	301	4
8	575.4	391.2	1.47	0.05281	0.00414	0.13485	0.01011	0.01852	0.00037	321	134	128	9	118	2
9	428.6	436.4	0.98	0.04776	0.00325	0.12901	0.00834	0.01959	0.00034	87	111	123	8	125	2

(*Continued*)

Table 3: Continued

Spots	(ppm) Th	U	Th/U	Isotopic ratios $^{207}Pb/^{206}Pb$	±1σ	$^{207}Pb/^{235}U$	±1σ	$^{206}Pb/^{238}U$	±1σ	Ages (Ma) $^{207}Pb/^{206}Pb$	±1σ	$^{207}Pb/^{235}U$	±1σ	$^{206}Pb/^{238}U$	±1σ
10	258.1	242.5	1.06	0.05991	0.01361	0.13728	0.0309	0.01662	0.00052	600	473	131	28	106	3
11	862.6	530.5	1.63	0.04883	0.00293	0.12869	0.00726	0.01911	0.00031	140	98	123	7	122	2
12	123.9	392.2	0.32	0.0493	0.00331	0.12596	0.00803	0.01853	0.00032	162	113	120	7	118	2
13	687.9	354.6	1.94	0.0461	0.0026	0.12233	0.00646	0.01924	0.00029	3	84	117	6	123	2
14	609.5	396.4	1.54	0.0715	0.00472	0.19773	0.01225	0.02005	0.00039	972	95	183	10	128	2
15	1037	552.2	1.88	0.04988	0.00251	0.13493	0.00627	0.01962	0.00029	189	81	129	6	125	2
16	1935	913.8	2.12	0.04901	0.00259	0.13179	0.00646	0.0195	0.00029	148	85	126	6	124	2
17	167	147.3	1.13	0.04614	0.00848	0.12726	0.02293	0.02	0.00071	5	272	122	21	128	4
18	149.3	222.9	0.67	0.04758	0.00488	0.12929	0.01283	0.01971	0.00046	78	176	123	12	126	3
19	191.4	209	0.92	0.05055	0.00511	0.1324	0.01291	0.01899	0.00046	220	175	126	12	121	3
20	751.5	482.5	1.56	0.04673	0.00312	0.12607	0.00797	0.01957	0.00033	35	105	121	7	125	2
TZ1607B1															
1	85.49	602.6	0.14	0.04906	0.00253	0.1305	0.00619	0.01929	0.00027	151	83	125	6	123	2
2	346.2	514	0.67	0.15752	0.00347	3.84468	0.04807	0.17698	0.00186	2429	10	1602	10	1050	10
3	89.85	371.9	0.24	0.05212	0.00315	0.1332	0.00751	0.01853	0.0003	291	99	127	7	118	2
4	94.02	686.9	0.14	0.05192	0.00244	0.13392	0.0057	0.0187	0.00026	282	72	128	5	119	2
5	126.7	578.1	0.22	0.04966	0.0024	0.13151	0.00578	0.0192	0.00026	179	77	125	5	123	2
6	135.6	642.1	0.21	0.04863	0.00164	0.12812	0.00361	0.0191	0.00022	130	45	122	3	122	1
7	120.9	818.7	0.15	0.04703	0.00211	0.1268	0.00512	0.01955	0.00026	51	64	121	5	125	2
8	144.9	741.1	0.20	0.04894	0.00173	0.13055	0.00392	0.01934	0.00023	145	48	125	4	123	1
9	73.3	520.4	0.14	0.04716	0.00281	0.1283	0.00717	0.01972	0.00031	57	93	123	6	126	2
10	162.9	716	0.23	0.04781	0.00197	0.12929	0.00471	0.01961	0.00025	90	60	123	4	125	2
11	33.72	309	0.11	0.04792	0.00378	0.12873	0.00971	0.01948	0.00037	95	132	123	9	124	2
12	30.68	397	0.08	0.04804	0.00315	0.1288	0.00798	0.01944	0.00032	101	107	123	7	124	2
13	142	396.9	0.36	0.10099	0.00381	2.29012	0.08069	0.16447	0.0022	1642	72	1209	25	982	12
14	95.68	340.5	0.28	0.0898	0.00289	0.39559	0.01038	0.03194	0.00041	1421	31	338	8	203	3
15	81.63	653.8	0.12	0.04975	0.00266	0.13201	0.00653	0.01924	0.00029	183	87	126	6	123	2
16	117.2	809.8	0.14	0.04619	0.00209	0.1257	0.00515	0.01973	0.00027	8	60	120	5	126	2
17	47.03	460.7	0.10	0.05175	0.00319	0.13499	0.00805	0.01892	0.0003	274	143	129	7	121	2
18	73.36	656.7	0.11	0.04712	0.00324	0.12819	0.00835	0.01973	0.00035	55	109	122	8	126	2
19	113.6	755.1	0.15	0.04996	0.00274	0.13184	0.00672	0.01914	0.00029	193	90	126	6	122	2

(*Continued*)

Table 3: Continued

	(ppm)			Isotopic ratios						Ages (Ma)					
Spots	Th	U	Th/U	$^{207}Pb/^{206}Pb$	±1σ	$^{207}Pb/^{235}U$	±1σ	$^{206}Pb/^{238}U$	±1σ	$^{207}Pb/^{206}Pb$	±1σ	$^{207}Pb/^{235}U$	±1σ	$^{206}Pb/^{238}U$	±1σ
20	43.42	429.7	0.10	0.0545	0.00392	0.14476	0.00988	0.01927	0.00036	392	120	137	9	123	2
JX1602B1															
1	318.9	737	0.43	0.16818	0.00358	10.7895	0.1234	0.46522	0.00483	2540	9	2505	11	2463	21
2	446.2	309	1.44	0.16839	0.00366	11.203	0.13966	0.48244	0.00522	2542	9	2540	12	2538	23
3	67.28	83	0.81	0.1679	0.00383	11.1234	0.16095	0.4804	0.00562	2537	11	2534	13	2529	24
4	266	440	0.60	0.16948	0.0038	8.51746	0.11644	0.36441	0.0041	2553	10	2288	12	2003	19
5	175.6	519	0.34	0.05008	0.0024	0.1333	0.00582	0.0193	0.00027	199	75	127	5	123	2
6	97.95	144	0.68	0.04605	0.00249	0.11794	0.0059	0.01858	0.00038	-	117	113	5	119	2
7	268.1	829	0.32	0.05247	0.0034	0.13653	0.00858	0.01887	0.0003	306	150	130	8	121	2
8	197.3	687	0.29	0.04863	0.00259	0.12749	0.00629	0.01901	0.00028	130	85	122	6	121	2
9	140.7	511	0.28	0.04854	0.00327	0.12784	0.00815	0.0191	0.00033	126	111	122	7	122	2
10	83.07	132	0.63	0.16889	0.00374	9.65015	0.13043	0.41427	0.0047	2547	10	2402	12	2234	21
11	78.4	169	0.46	0.05975	0.00626	0.15552	0.01569	0.01887	0.00049	595	175	147	14	121	3
12	188.6	629	0.30	0.04846	0.00245	0.12728	0.00591	0.01904	0.00027	122	80	122	5	122	2
13	151.2	504	0.30	0.04846	0.00373	0.1285	0.00945	0.01923	0.00037	122	128	123	9	123	2
14	177.6	159	1.12	0.16696	0.00408	11.0666	0.19591	0.4806	0.00643	2527	14	2529	16	2530	28
15	88.08	285	0.31	0.16763	0.00385	10.4684	0.16043	0.45283	0.00555	2534	12	2477	14	2408	25
16	33.08	123	0.27	0.16743	0.00385	10.2565	0.15767	0.44422	0.00546	2532	12	2458	14	2370	24
17	6.99	9	0.78	0.16785	0.01207	11.3853	0.83873	0.49189	0.02182	2536	67	2555	69	2579	94
18	75.67	317	0.24	0.0589	0.00435	0.16024	0.01124	0.01973	0.00039	563	119	151	10	126	2
19	211	333	0.63	0.16736	0.00369	10.985	0.15287	0.47601	0.0056	2531	10	2522	13	2510	24
20	179.6	604	0.30	0.0501	0.00282	0.13195	0.00692	0.0191	0.0003	200	92	126	6	122	2
JX1603B1															
1	77.44	226	0.34	0.16936	0.00418	8.92702	0.1532	0.38196	0.00488	2551	14	2331	16	2085	23
2	118.6	576	0.21	0.04784	0.00363	0.12271	0.00888	0.01859	0.00035	91	125	118	8	119	2
3	201.9	679	0.30	0.0487	0.00187	0.13102	0.00436	0.0195	0.00024	133	55	125	4	124	2
4	50.96	288	0.18	0.04863	0.00438	0.13092	0.01133	0.01951	0.00042	130	153	125	10	125	3
5	421.8	950	0.44	0.04903	0.00256	0.1276	0.00615	0.01886	0.00028	149	83	122	6	120	2
6	45.83	228	0.20	0.04808	0.00308	0.12421	0.00752	0.01872	0.00031	103	104	119	7	120	2
7	326.9	828	0.39	0.04893	0.00182	0.12741	0.0041	0.01887	0.00024	144	52	122	4	121	2
8	76.42	184	0.42	0.0485	0.00481	0.12564	0.01203	0.01877	0.00043	124	170	120	11	120	3

(*Continued*)

Table 3: Continued

Spots	(ppm) Th	U	Th/U	Isotopic ratios $^{207}Pb/^{206}Pb$	±1σ	$^{207}Pb/^{235}U$	±1σ	$^{206}Pb/^{238}U$	±1σ	Ages (Ma) $^{207}Pb/^{206}Pb$	±1σ	$^{207}Pb/^{235}U$	±1σ	$^{206}Pb/^{238}U$	±1σ
9	696.2	826	0.84	0.05013	0.00196	0.12917	0.00443	0.01867	0.00024	201	56	123	4	119	2
10	139.3	529	0.26	0.0473	0.00209	0.12556	0.00502	0.01924	0.00026	64	64	120	5	123	2
11	234	750	0.31	0.04876	0.00253	0.12764	0.00614	0.01898	0.00028	136	83	122	6	121	2
12	21.24	119	0.18	0.04851	0.00634	0.12878	0.01638	0.01925	0.00055	124	228	123	15	123	3
13	87.58	398	0.22	0.04904	0.00319	0.1253	0.00772	0.01853	0.00032	150	107	120	7	118	2
14	53.6	84	0.64	0.16472	0.0043	10.7771	0.22367	0.47462	0.00714	2505	17	2504	19	2504	31
15	186.4	688	0.27	0.05228	0.00288	0.13098	0.00673	0.01818	0.00029	298	88	125	6	116	2
16	88.75	427	0.21	0.04857	0.00317	0.12441	0.0077	0.01859	0.00032	127	107	119	7	119	2
17	196.6	563	0.35	0.04948	0.0035	0.13257	0.00893	0.01945	0.00036	171	118	126	8	124	2
18	31.4	75	0.42	0.16362	0.00387	10.7766	0.18938	0.47826	0.00653	2493	14	2504	16	2520	28
19	278.4	787	0.35	0.04928	0.00226	0.12755	0.00536	0.0188	0.00027	161	71	122	5	120	2
20	21.13	145	0.15	0.06056	0.00837	0.15033	0.02013	0.01803	0.00062	624	234	142	18	115	4
SSY1601B1															
1	180.7	762.8	0.24	0.05369	0.00285	0.14514	0.00712	0.0196	0.0003	358	83	138	6	125	2
2	124.9	795.2	0.16	0.04636	0.00257	0.12485	0.00645	0.01953	0.00029	16	82	119	6	125	2
3	350.3	914.9	0.38	0.04674	0.00179	0.12544	0.00421	0.01946	0.00024	36	50	120	4	124	2
4	145.2	663.4	0.22	0.04946	0.00217	0.13172	0.00519	0.01931	0.00026	170	67	126	5	123	2
5	90.94	570.5	0.16	0.05074	0.00312	0.13554	0.00783	0.01937	0.00032	229	103	129	7	124	2
6	64.88	360.7	0.18	0.04804	0.00371	0.14354	0.01059	0.02167	0.00041	101	128	136	9	138	3
7	155.9	777.7	0.20	0.04812	0.00177	0.12984	0.00412	0.01956	0.00024	105	52	124	4	125	2
8	42.28	342.2	0.12	0.04775	0.00225	0.12919	0.00554	0.01962	0.00027	87	71	123	5	125	2
9	129.2	668.6	0.19	0.04747	0.00308	0.12745	0.0078	0.01947	0.00032	73	104	122	7	124	2
10	187	873.4	0.21	0.05393	0.00246	0.14348	0.00628	0.01929	0.00025	368	105	136	6	123	2
11	155.3	731.5	0.21	0.0477	0.00164	0.12869	0.00375	0.01957	0.00023	84	46	123	3	125	1
12	111.9	567.3	0.20	0.04792	0.00244	0.12931	0.00608	0.01957	0.00028	95	79	123	5	125	2
13	210.8	658.9	0.32	0.047	0.00162	0.12569	0.00366	0.01939	0.00023	49	44	120	3	124	1
14	192.8	792.6	0.24	0.05246	0.00305	0.14003	0.0076	0.01936	0.00031	306	95	133	7	124	2
15	92.15	570.4	0.16	0.04657	0.00179	0.12576	0.00424	0.01958	0.00024	27	50	120	4	125	2
16	140	372.7	0.38	0.04833	0.00225	0.13075	0.00556	0.01962	0.00026	115	73	125	5	125	2
17	75.91	518.7	0.15	0.04674	0.00208	0.12578	0.00506	0.01952	0.00026	36	62	120	5	125	2
18	170.6	468.2	0.36	0.04775	0.00194	0.12753	0.00461	0.01937	0.00024	87	60	122	4	124	2

(*Continued*)

Table 3: Continued

Spots	(ppm) Th	U	Th/U	Isotopic ratios $^{207}Pb/^{206}Pb$	±1σ	$^{207}Pb/^{235}U$	±1σ	$^{206}Pb/^{238}U$	±1σ	Ages (Ma) $^{207}Pb/^{206}Pb$	±1σ	$^{207}Pb/^{235}U$	±1σ	$^{206}Pb/^{238}U$	±1σ
19	109	699.7	0.16	0.04849	0.0017	0.13055	0.00389	0.01952	0.00023	123	48	125	3	125	1
20	168	674.9	0.25	0.04862	0.00189	0.1312	0.00449	0.01957	0.00024	130	57	125	4	125	2
SSY1601B2															
1	159.2	718	0.22	0.04839	0.00239	0.12946	0.00587	0.01939	0.00027	118	78	124	5	124	2
2	105.9	563	0.19	0.0483	0.00182	0.12883	0.00423	0.01934	0.00024	114	54	123	4	123	2
3	331.7	663	0.50	0.04763	0.00171	0.12864	0.00394	0.01958	0.00023	81	50	123	4	125	1
4	161.1	736	0.22	0.04848	0.00289	0.13006	0.00726	0.01945	0.00031	123	96	124	7	124	2
5	255.1	809	0.32	0.04771	0.00201	0.12678	0.00476	0.01927	0.00025	85	61	121	4	123	2
6	161	778	0.21	0.05088	0.0027	0.13275	0.00651	0.01892	0.00028	235	86	127	6	121	2
7	106.2	613	0.17	0.04923	0.00217	0.12849	0.0051	0.01893	0.00025	159	68	123	5	121	2
8	80.09	447	0.18	0.04749	0.00254	0.13015	0.00645	0.01987	0.00029	74	82	124	6	127	2
9	161.1	725	0.22	0.0478	0.00254	0.12815	0.0063	0.01944	0.00028	89	83	122	6	124	2
10	135.4	774	0.17	0.05048	0.00307	0.13219	0.00753	0.01899	0.00031	217	101	126	7	121	2
11	110.2	342	0.32	0.04952	0.00332	0.13094	0.00831	0.01918	0.00032	173	114	125	7	122	2
12	100.2	596	0.17	0.04707	0.00216	0.12797	0.00531	0.01972	0.00026	53	66	122	5	126	2
13	245.9	904	0.27	0.04905	0.00206	0.13199	0.00493	0.01952	0.00025	150	63	126	4	125	2
14	253.1	842	0.30	0.0499	0.00205	0.12958	0.00469	0.01883	0.00024	190	60	124	4	120	2
15	209.1	774	0.27	0.04988	0.00269	0.13165	0.00657	0.01914	0.00028	189	89	126	6	122	2
16	106	723	0.15	0.04979	0.00263	0.13195	0.00641	0.01922	0.00028	185	86	126	6	123	2
17	121	639	0.19	0.04941	0.00289	0.13127	0.00717	0.01927	0.0003	167	96	125	6	123	2
18	115.2	671	0.17	0.04886	0.00228	0.12676	0.00536	0.01882	0.00026	141	73	121	5	120	2
19	145.3	459	0.32	0.05283	0.0044	0.1324	0.01054	0.01817	0.00037	322	144	126	9	116	2
20	126.2	617	0.20	0.04808	0.00354	0.12836	0.00899	0.01936	0.00035	103	122	123	8	124	2
SSY1602B1															
1	92.6	581.6	0.16	0.04836	0.00255	0.13002	0.00638	0.01949	0.00029	117	84	124	6	124	2
2	149.4	780.2	0.19	0.0473	0.00241	0.12905	0.0061	0.01978	0.00029	64	77	123	5	126	2
3	144.7	668.2	0.22	0.04842	0.00251	0.12941	0.00622	0.01938	0.00029	120	82	124	6	124	2
4	109.4	806.4	0.14	0.04734	0.00247	0.12683	0.00615	0.01943	0.00029	66	79	121	6	124	2
5	147.7	693	0.21	0.04852	0.00262	0.12974	0.00652	0.01939	0.0003	125	86	124	6	124	2
6	47.04	445.1	0.11	0.04633	0.00356	0.1245	0.00916	0.01948	0.00037	15	125	119	8	124	2
7	53.79	266.7	0.20	0.04616	0.00397	0.12457	0.01033	0.01957	0.00038	6	145	119	9	125	2

(*Continued*)

Table 3: Continued

	(ppm)			Isotopic ratios						Ages (Ma)					
Spots	Th	U	Th/U	$^{207}Pb/^{206}Pb$	±1σ	$^{207}Pb/^{235}U$	±1σ	$^{206}Pb/^{238}U$	±1σ	$^{207}Pb/^{206}Pb$	±1σ	$^{207}Pb/^{235}U$	±1σ	$^{206}Pb/^{238}U$	±1σ
8	71.67	423.8	0.17	0.04702	0.00327	0.12732	0.00845	0.01964	0.00035	50	111	122	8	125	2
9	153.2	754.1	0.20	0.04538	0.00315	0.12331	0.00815	0.0197	0.00035	-	109	118	7	126	2
10	259.1	593.7	0.44	0.04854	0.00305	0.13028	0.00772	0.01946	0.00033	126	102	124	7	124	2
11	94.5	584.1	0.16	0.05188	0.00315	0.13638	0.0078	0.01906	0.00032	280	100	130	7	122	2
12	127.3	642.6	0.20	0.06091	0.00361	0.16094	0.00913	0.01916	0.00033	636	131	152	8	122	2
13	180.7	484.9	0.37	0.05009	0.00347	0.13034	0.00858	0.01887	0.00034	199	117	124	8	121	2
14	112.6	801.6	0.14	0.05201	0.00332	0.13227	0.00797	0.01844	0.00032	286	106	126	7	118	2
15	226	1098	0.21	0.04682	0.00234	0.12387	0.00573	0.01918	0.00028	40	73	119	5	122	2
16	148.7	796	0.19	0.04637	0.00236	0.12413	0.00584	0.01941	0.00028	17	73	119	5	124	2
17	59.88	398.9	0.15	0.04788	0.00383	0.12595	0.00967	0.01907	0.00037	93	134	120	9	122	2
18	163.5	850.9	0.19	0.04788	0.00265	0.12725	0.00657	0.01927	0.0003	93	86	122	6	123	2
19	61.03	450.6	0.14	0.04735	0.00387	0.1244	0.00975	0.01905	0.00038	67	135	119	9	122	2
20	71.02	556.6	0.13	0.04683	0.00251	0.12447	0.00621	0.01927	0.00029	41	80	119	6	123	2

4.4. Lu-Hf Isotopes. Eight dated samples were also analyzed for Lu-Hf isotope compositions within the same dated zircon domains. The REE zircon data of samples are shown in Table 4. The analytical results and calculation parameters are listed in Table 5. The $f_{Lu/Hf}$ values of all the analysis spots concentrate on −0.95, which is lower than those of the mafic lower crust with a value of −0.34 and felsic upper crust with a value of −0.72 [63]. The $^{176}Lu/^{177}Hf$ analyses are <0.002.

When corrected to their respective magmatic crystallization ages, all these samples show ε_{Hf} (t_1) values close to the (CHUR) evolution line (Figure 8). The diorites (sample JX1602B1 and JX16D03B1) show ε_{Hf} (t_1= 120–125 Ma) values from −9.1 to 0.9 with T_{DM}^C ages of 1674–1733 Ma and ε_{Hf} (t_2= 2505–2539 Ma) 2.5–4.6 with T_{DM}^C ages of 2676–2756 Ma. The diorites (Sample TZ16D03B2 and TZ16D04B2) yield $\varepsilon_{Hf}(t_1)$ values between −0.9 and 7.8 with (T_{DM}^C) of 658–1206 Ma. Analogously, the syenite porphyry (Sample SSYD01B1, SSYD01B2, and Sample TZ16D07B1) and monzonite (Sample SSY16D02B1) show ε_{Hf} (t_1) values from −5.2 to 0.5 with T_{DM}^C ages of 745–1645 Ma. And two spots of (Sample TZ16D07B1) yield ε_{Hf} (t_1) values of −25.5 and −25.6.

5. Discussion

5.1. Petrogenesis

5.1.1. Magma Mixing Between Mafic and Felsic Melts. The Jinxingtou, Tiezhai, and Sanshanyu complexes possess similar geochronological, geological, and petrological features, suggesting that they are comagmatic and formed in the same tectonic thermal event [20, 56, 58]. Crustal assimilation and fractional crystallization may occur synchronously during magma ascent [47]. Among the zircon grains of these "High Sr/Y granitoids" in Luxi Terrane, inherited zircon cores from basement rocks of NCC might suggest the presence of crustal contamination during magma ascent [6]. The involvement of continental components is also indicated by the crust-like trace element features, including enrichment in LILEs and LREEs, positive Pb anomalies and depletion in HFSEs, and negative Nb-Ta anomalies. However, the high Sr (480, 1107 ppm) and Ba (445, 1282 ppm) preclude any significant input of crustal components. In addition, higher Lu/Yb ratios (0.16, 0.18) are considered as an indicator of crustal involvement [64], whereas our data display only a lower range of 0.14–0.15 indicating minor effects of crustal contamination.

Now we consider the fractional crystallization process which is another important factor. In the Harker diagram, the major elements of the samples display a trend of fractional crystallization process (Figure 9). This is consistent with the mantle-derived amphibole enclaves in the Luxi Terrane [65]. The amphibole-bearing cumulates within the MMEs are most likely to be homologous with the host rock and derived from the fractional crystallization of diorite magma in the magma chamber [20, 56, 65, 66]. Based on petrography and geochemical characteristics, previous studies indicate that parental magma of the Early Cretaceous intrusions may have been sourced from the partial melting of the enriched mantle and the assimilation of some ancient crustal materials [14, 19, 20, 23, 35, 56, 67]. However, several lines of evidence lead us to support that these "High Sr/Y granitoids" in the Luxi Terrane could have been formed by magma mixing/mingling of the basic and felsic end-members [4].

(1) Plagioclase mineral evidence. Crystallization within a closed system cannot lead to structural disequilibrium observed in plagioclases of these "High Sr/Y granites" (Figure 4(d)). The overgrowth rim can be observed in the samples, suggesting the reaction between silicic and relatively mafic magma [68]. In addition, quartz monzonite in the Tiezhai Complex containing plagioclase phenocrysts featured by compositional zoning with high Ca content in the core (~31 An%) and contrasting low Ca content in the rim zone (~18 An%) [20, 56]. The plagioclase cores are interpreted as relict An-rich plagioclase grains initially in equilibrium with the gabbronoritic magma.

(2) Major element evidence. A high $Mg^{\#}$ value (49–73) is a useful parameter for discriminating purely crust-derived magma from those that have involved the mantle-derived component [4, 68]. The Mg numbers of the adakitic rocks of the Luxi Terrane, regardless of high- or low-SiO_2 variety, are basically higher than those of experimental melts from basalts at the same silica contents (Figures 10(a) and 10(b) [36]). Therefore, a sole thickened mafic lower crust source is unreasonable, and the addition of high-Mg lithospheric mantle-derived mafic magma is required. Few adakite samples with relatively low $Mg^{\#}$ content such as monzonite (TZ16D07B1, $Mg^{\#}$ = 37) were considered to be the result of crystallization differentiation of magnetite [20, 56]. In addition, the increasing Fe + Mg contents would be expected due to the basification of relatively felsic magma [69]. In this study, the positive correlation of FeOT + MgO and TiO_2 contents is also in favor of magma mixing between mantle-derived mafic magma and crust-derived felsic melts (Figure 6(d); [70]).

(3) Trace element evidence. The "High Sr/Y granitoids" in the Luxi Terrane display limited fractionated LREE patterns relative to MREE ($[La/Sm]_N$ = 2.19–3.90; Figure 6(f)), thus indicating the limited fractionation of MREE-enriched minerals (e.g., hornblende, clinopyroxene, and apatite) [71]. Eu anomaly is also of significance to trace the crustal evolution and exchange between crust and mantle [72]. They have negligible Eu anomalies in the REE patterns, suggesting mantle derived and insignificant plagioclase fractional crystallization in parental

Table 4: LA-ICP-MS analytical REE zircon data of samples from the Tiezhai, Jinxingtou, and Sanshanyu complexes in the Luxi Terrane.

	(ppm)															
Spots	La	Ce	Pr	Nd	Sm	Eu	Gd	Tb	Dy	Ho	Er	Tm	Yb	Lu	Y	Ti
TZD03B2																
1	248.27	493.33	46.78	172.29	32.88	13.4	38.27	8.41	81.73	28.35	129.02	29.3	307	62.38	11.81	69473.71
2	0.049	58.78	0.23	3.94	6.73	2.41	36.93	12.94	149.84	57.21	263.54	59.61	618.38	121.18	87.13	19.97
3	0.049	69.31	0.59	10.6	22.01	5.93	91.77	26.59	281.18	99.74	437.64	94.04	951.51	181.76	24.83	12.26
4	0.051	51.13	0.241	2.96	5.69	1.51	28.18	8.98	100.03	37.41	171.38	38.31	401.4	79.37	86.59	17.85
5	0.076	66.31	0.562	12.6	23.59	6.34	94.2	26.77	276.96	98.22	418.01	88.34	890.92	167.13	18.92	14.26
6	0.051	8.73	0.034	0.52	1.09	0.29	3.26	0.96	10.6	3.98	17.97	3.74	38.74	8.17	65.8	8.47
7	0.048	48.46	0.29	5.47	9.29	3.35	46.35	13.7	149.05	55.5	238.05	51.06	511.49	99.34	38.8	22.02
8	0.12	83.31	0.65	11.82	26.39	6.74	104.69	30.08	300.19	102.31	436.73	89.87	903.59	168.71	22.69	22.5
9	0.045	65.21	0.392	6.27	12.35	3.21	55.74	17.35	188.21	68.27	303.35	65.05	653.68	125.74	44.22	21.16
10	0.063	35.02	0.263	3.48	5.76	1.94	31.26	10.95	126.17	50.5	236.69	54.26	584.67	114.25	63.52	11.59
11	0.071	76.69	0.91	16.88	27.59	6.46	97.3	27.97	285.31	98.49	427.94	90.19	908.22	172.1	16.16	15.21
12	0.68	20.48	0.326	1.47	1.77	0.44	5.19	1.58	18.72	7.7	40.13	9.76	115.36	25.3	94.63	20.5
13	0.045	33.12	0.47	6.4	13.06	3.23	55.66	16.16	173.24	61.11	273.92	57.93	588.95	113.49	20.18	13.34
14	0.048	40.34	0.253	3.3	6.56	2.07	36.7	12.23	140.13	53.75	246.49	55.49	573.89	112.04	66.6	18.54
15	0.1	51.57	0.73	12.4	19.59	5.07	78.05	23.42	234.18	81.11	347.21	74.05	744.58	141.49	15.53	16.15
16	0.046	53.94	0.249	4.04	8.18	2.43	52.32	17.76	192.19	70.52	304.32	63.89	627.53	121.1	62.3	22.52
17	0.069	1.48	0.039	0.39	0.29	0.31	3.4	1.66	26.12	12.92	72.16	17.89	217.11	49.36	82.31	6.01
18	0.047	3.66	0.06	0.57	1.18	0.115	5.37	2.22	30.99	13.64	73.36	18.57	204.85	42.45	60.27	2.75
19	0.049	56.23	0.304	5.4	9.69	2.81	47.69	15.8	173.26	63.61	281.93	60.45	614.16	115.39	48.53	14.34
20	0.041	77.42	0.43	5.06	11.91	3.64	56.71	16.72	189.17	67.02	290.49	63.29	625.82	120.57	61.24	23.33
TZD04B2																
1	0.61	63.03	0.885	14.16	25.57	5.86	104.42	31.6	325.68	113.34	476.34	96.69	923.49	163.79	15.24	7.51
2	0.046	16.01	0.087	1.45	3.72	0.87	19.99	6.93	79.73	30.97	145.09	31.82	329.63	62.97	57.7	5.69
3	0.081	82.58	0.91	14.19	26.66	5.41	107.86	32.61	345.94	119.7	505.22	102.68	969.2	168.43	19.85	5.68
4	0.042	35.89	0.147	2.16	4.67	1.26	24.78	8.05	90.91	35.32	153.86	32.37	320.75	58.46	76.23	7.47
5	0.038	47.29	0.52	7.86	15.04	3.47	66.17	20.17	216.34	76.76	325.26	67.44	641.92	114.55	22.18	7.75
6	0.179	82.79	1.16	17.75	34.68	8.78	156.3	47.75	490.27	167.6	685.73	138.81	1311.96	221.36	15.28	9.3
7	0.114	37.68	0.5	8.64	15.24	3.46	60.47	18.18	189.6	66.11	276.32	57.76	553.76	94.53	15.1	13.06
8	0.083	52.37	0.509	8.43	14.75	3.7	70.15	21.82	233.16	80.72	342.75	72.73	706.81	117.81	23.82	9.44
9	0.053	38.78	0.185	2.92	7.66	1.84	41.49	13.49	162.44	62.42	281.46	63.31	644.89	114.58	65.73	6.11

(*Continued*)

Table 4: Continued

Spots	La	Ce	Pr	Nd	Sm	Eu	Gd	Tb	Dy (ppm)	Ho	Er	Tm	Yb	Lu	Y	Ti
10	0.072	29.76	0.342	6.26	10.48	2.14	44.47	14.12	152.92	53.85	231.4	50.35	487.98	82.66	19.01	4.99
11	0.146	70.64	0.92	15.04	25.93	5.97	118.01	36.23	376.08	131.11	545.65	112.58	1072.24	181.81	16.79	7.66
12	0.043	19.61	0.038	0.69	1.51	1.02	8.9	3.21	42.02	17.04	84.4	20.49	228.91	48.31	217.47	2.85
13	0.061	50.86	0.74	11.49	22.62	5.62	98.9	29.51	310.34	105.39	425.24	86.54	813.63	138.93	14.25	9.93
14	0.351	41.44	0.444	6.95	12.04	2.98	59.57	19.43	215.97	77.32	329.33	68.77	656.21	115.53	24.99	31.79
15	0.18	83.72	1.14	19.62	34.78	8.73	153.31	46.65	477.98	160.8	664.54	134.46	1267.28	214.63	14.08	8.91
16	0.266	194.7	2.02	37.2	71.53	16.57	288.1	83.51	827.56	270.08	1053.71	207.12	1866.27	293.77	13.84	9.88
17	0.173	19.51	0.3	4.39	7.97	1.99	31.37	10.69	115.55	41.12	176.44	36.82	368.39	65.17	17.86	39.22
18	0.054	20.78	0.157	1.9	5.56	1.09	22.87	7.34	84.8	31.89	141.36	31.27	315.66	55.69	45.15	4.67
19	0.051	22.09	0.291	4.98	8.06	2.27	35.39	11.1	119.32	42.81	182.97	39.35	385.22	69.56	18.28	5.84
20	0.089	62.34	0.82	13.08	23.27	5.82	109.31	33.96	362.95	124.79	517.11	107.02	1041.79	171.81	17.38	7.72
TZD07B1																
1	0.055	6.92	0.034	0.66	1.14	0.75	6.58	2.18	22.72	8.53	42.21	9.43	112.16	23.53	63	1.99
2	0.196	28.97	0.202	1.32	1.94	0.78	7.84	2.32	25.58	9.86	48.48	12.11	140.9	30.14	132.57	9.02
3	0.076	8.07	0.043	0.56	0.86	0.58	4.69	1.62	18.68	6.97	34.67	8.5	91.91	19.63	97.89	4.51
4	0.039	6.08	0.018	0.44	1.15	0.83	6.1	1.84	21.07	8.23	39.72	9.59	110.92	23.74	79.21	1.71
5	0.101	10.99	0.062	0.58	1.75	1.16	10.98	3.42	38.69	14.07	67.31	16	174.2	35.43	98.63	2.26
6	0.063	12.54	0.049	0.77	1.8	1.41	11.49	3.72	42.34	16	76.95	18.2	201.04	41.41	96.45	2.57
7	0.061	7.95	0.024	0.41	1.9	1.44	12.51	4.09	42.98	15.88	72.75	16.57	186.96	36.91	86.85	3.17
8	41.53	179.26	31.53	166.46	41.85	12.39	35.83	5.45	34.99	9.02	37.27	8.06	87.46	18.42	1.74	23135.97
9	28.19	119.13	19.8	101.96	23.02	7.3	20.02	3.6	28.12	8.96	42.08	10.35	118.57	24.85	3.53	11225.6
10	0.06	11.75	0.033	0.56	2.11	1.51	11.94	3.85	42.33	16.12	76.28	17.54	195.34	38.99	102.01	2.68
11	0.046	5.45	0.025	0.34	0.99	0.79	7.18	2.3	26.99	11.51	59.28	14.72	170.13	37.25	117.91	2.1
12	0.022	6.12	0.046	0.46	2.16	1.36	14.21	5.51	60.42	22.41	99.99	23.33	247.14	49.79	65.23	2.22
13	0.037	9.45	0.074	0.97	2.06	0.58	9.77	2.7	25.86	8.71	36.02	7.73	81.45	14.94	32.1	9.35
14	0.045	10.32	0.028	0.38	0.98	0.78	6.91	2.26	25.3	9.97	47.88	11.67	127.87	25.7	167.11	2.68
15	0.038	7.15	0.033	0.44	1.21	0.87	6.85	2.14	24.91	9.17	44.57	10.88	129.38	26.14	93.26	1.43
16	0.042	7.38	0.027	0.41	1.08	0.89	7.21	2.12	22.84	8.25	39.63	9.37	106.26	22.09	94.03	13.57
17	0.06	6.41	0.07	0.53	1.28	0.81	5.88	1.94	21.24	7.47	33.45	7.95	85.57	17.02	56.29	2.06
18	0.102	7.31	0.053	0.59	1.44	0.75	8.05	2.74	31.47	12.29	57.98	13.56	149.19	30.66	72.55	1.49
19	4.42	28.43	3.51	19.42	5.7	2.41	11.62	3.19	31.27	11.26	51.74	12.08	133.25	27.21	7.81	2458.21

(*Continued*)

Table 4: Continued

	(ppm)															
Spots	La	Ce	Pr	Nd	Sm	Eu	Gd	Tb	Dy	Ho	Er	Tm	Yb	Lu	Y	Ti
20	0.044	7.04	0.043	0.35	1.3	0.88	8.18	3	30.63	12.29	58.03	14.15	157.66	32.65	112.13	2.91
JXD02B1																
1	0.352	24.35	0.13	1.36	1.35	0.534	7.08	2.65	33.43	13.88	70.68	17.57	200.23	41.66	168.23	25.7
2	0.035	68.42	0.183	4.44	8.17	1	40	13.46	159.12	61.45	279.55	60.83	590.82	104.93	78.13	7.31
3	0.052	10.73	0.428	6.19	8.66	1.17	27.54	8.47	86.43	29	120.27	24.27	227.97	40.1	5.59	14.67
4	0.56	23.69	0.79	7.58	6.03	2.39	15.76	5.56	52.36	16.75	67.65	14.19	140.41	26.29	11.23	19.27
5	0.056	14.83	0.031	0.73	1.86	1.28	12.89	4.07	45.65	16.96	75.63	17.13	173.12	33.3	100.01	2.41
6	0.337	9.37	0.229	3.41	4.3	2.07	17.11	5.11	52.69	19.53	89.67	19.86	216.47	44.23	13.33	14.63
7	0.022	24.9	0.09	1.21	4.69	2.76	26.13	8.34	92.32	35.17	158.42	34.93	353.98	64.97	86.34	4.64
8	0.035	26.03	0.048	1.18	4.52	2.79	23.89	8.36	94.22	35.82	163.15	37.13	379.82	69.22	100.4	4.03
9	0.021	19.22	0.047	0.64	2.4	1.75	16.98	6.09	71.53	27.78	126.09	27.7	283.96	51.18	152.99	3.51
10	0.208	12.19	0.153	1.64	3.15	0.316	13.84	4.21	47.25	16.98	73.37	14.89	145.66	25.97	28.9	9.57
11	0.033	8.81	0.066	1.08	2.16	1.24	10.5	3.58	45.42	19.58	94.79	22.17	245.52	51.24	57.33	4.48
12	0.063	22.06	0.038	0.81	3.42	2.24	21.19	7.18	83.77	31.55	142.72	32.05	329.66	60.11	125	3.82
13	0.046	14.64	0.035	0.65	2.15	1.52	12.47	4.29	47.58	17.61	81.51	18.25	188.9	34.61	105.21	2.46
14	0.066	25.58	0.178	2.77	5.6	0.25	20.7	6.97	74.08	25.08	102.7	20.77	190.24	34.23	30.55	13.92
15	0.067	17.39	0.045	0.72	0.96	0.197	4.84	1.83	23.73	9.39	49.5	12.78	143.8	28.8	214.6	9.84
16	0.044	20.4	0.075	1.16	2.01	0.295	10.33	3.49	39.83	14.74	66.43	14.49	148.43	26.68	88.81	13.1
17	0.038	11.98	0.064	1.28	1.61	0.75	7.91	2.01	19.22	6.62	27.57	5.84	57.19	9.41	31.78	23.72
18	0.46	10.76	0.11	0.88	1.64	1.1	9.97	3.3	38.16	14.66	69.99	15.66	166.4	31.96	71.92	3.9
19	0.043	30.43	0.155	0.68	1.18	0.237	6.53	2.44	30.88	11.53	54.95	13.74	157.67	30.75	325.87	7.21
20	0.046	20.48	0.023	0.74	3	1.86	19.04	6.32	69.46	26.97	121.92	27.73	276.77	50.34	124.31	4.12
JXD03B1																
1	0.073	17.77	0.069	0.85	1.29	0.321	5.78	2	24.25	9.53	44.7	10.32	105.22	21.06	127.77	5.42
2	0.021	19.69	0.031	1	3.48	1.99	19.68	6.91	82.32	32	149.04	34.32	346.39	66.11	101.88	3.52
3	0.04	21.49	0.054	1.01	3.58	2.15	19.35	6.34	72.58	27.33	126.26	27.9	283.27	53.61	95.84	3.36
4	0.048	13.01	0.028	0.54	2.94	1.75	17.17	6.54	81.31	32.74	154.53	34.86	363.82	69.57	127.26	3.51
5	0.049	23.06	0.039	1.12	4.03	2.05	17.81	6.12	69.87	25.19	117.36	25.6	272.61	48.64	87.25	4.79
6	0.193	8.1	0.081	0.42	1.14	0.72	7.76	2.64	30.9	12.73	61.38	13.72	142.24	28.4	116.43	1.58
7	0.036	27.21	0.033	1.23	4.16	2.4	22.53	7.27	81.85	30.21	135.59	29.05	291.48	54.22	92.23	3.6
8	0.043	7.64	0.069	1.03	1.7	0.82	6.88	2.55	32.32	14.15	64.88	17.07	178.99	35.92	54.81	3.15

(*Continued*)

Table 4: Continued

Spots	(ppm) La	Ce	Pr	Nd	Sm	Eu	Gd	Tb	Dy	Ho	Er	Tm	Yb	Lu	Y	Ti
9	0.088	28.62	0.319	3.82	6.38	3.99	34.21	11.22	125.49	45.85	203.22	43.56	441.77	86.03	36.81	3.91
10	0.044	18.09	0.042	0.71	2.81	1.86	16.9	5.89	70.01	27.41	127.36	28.65	290.64	55.3	128.09	4.93
11	0.052	26.79	0.038	1.01	4.46	2.55	24.32	8.15	89.07	34.12	150.84	32.49	334.15	58.99	106.16	4.77
12	0.022	6.21	0.036	0.27	0.75	0.53	4.69	1.81	25.1	10.38	51.39	12.3	133.61	25.3	175.83	2.3
13	0.137	14.33	0.057	0.51	2.67	1.39	14.82	4.87	57.17	22.21	102.24	23.97	241.95	44.86	125.19	4.01
14	0.031	16.29	0.056	0.7	1.69	0.33	8.06	2.75	32.44	12.08	55.45	12.05	118.93	22.39	110.97	10.55
15	0.013	23.17	0.056	1.27	3.27	1.99	21.22	6.53	75.96	27.98	129.73	28.83	303.04	54.53	90.16	3.57
16	0.034	12.4	0.03	0.44	1.45	0.94	9.83	3.56	45.34	17.49	83.18	18.69	194.17	35.5	164.49	2.25
17	0.065	17.04	0.047	0.86	2.48	1.74	15.23	4.97	59.78	22.38	103.51	22.77	233.36	41.63	98.2	3.12
18	0.018	7.56	0.033	0.54	1.43	0.52	5.73	2.12	26.86	10.78	54.7	12.98	145.65	30.96	91.65	13.79
19	0.058	28.71	0.035	1.31	3.81	2.38	21.98	7.85	87.36	33.79	150.36	33.59	338.82	61.18	106.13	5.65
20	0.073	6.06	0.036	0.48	1.54	0.98	9.29	3.31	39.89	15.52	74.1	18.07	181.51	35.4	73.14	1.98
SSYD01B1-1																
1	0.031	13.99	0.023	0.72	1.98	1.29	12.08	3.71	42.7	17.24	81.79	18.46	199.57	40.71	106.89	2.26
2	0.043	14.17	0.044	0.46	2.01	1.23	12.93	4.13	53.34	22.62	105.93	25.19	267.37	55.11	181.03	3.45
3	0.062	21.1	0.039	0.99	3.09	1.98	15.42	5.46	59.54	22.39	104.54	23.4	245.73	49.88	102.7	3.67
4	0.063	12.25	0.036	0.43	1.88	1.26	12.14	4.3	53.32	22.09	108.38	25.18	271.37	57.35	174.98	3.2
5	0.078	12.02	0.035	0.5	1.72	1.19	11.11	4.03	50.67	20.49	100.62	23.72	255.09	53.29	157.57	3.33
6	0.06	10.22	0.039	0.3	1.24	1.24	7.85	3.13	38.59	15.71	79.66	18.52	205.5	44.32	231.1	1.74
7	0.055	12.29	0.041	0.44	1.87	1.15	10.55	3.68	42.57	16.82	82.53	18.82	200.43	41.02	147.67	2.32
8	0.057	8.47	0.046	0.41	1.04	0.94	10.11	3.94	47.34	20.93	108.27	25.47	285.36	61.65	186.85	2.35
9	0.06	12.81	0.036	0.41	1.77	1.26	11.24	3.88	46.49	18.61	91.56	21.18	226.96	46.82	177.84	2.82
10	0.09	14.93	0.146	1.16	2.78	1.45	12.7	4.25	48.28	18.41	88.84	20.38	213.31	43.65	67.73	2.63
11	0.052	12.93	0.042	0.41	1.79	1.22	10.28	3.69	44.2	17.64	85.9	19.68	210.92	43.66	175.23	2.48
12	0.032	13.68	0.037	0.46	1.7	1.29	12.19	4.48	54.36	22.64	112.92	26.51	281.58	58.22	198.09	2.81
13	0.057	16.52	0.054	0.63	1.86	1.32	10.55	3.2	35.45	14.64	69.53	15.74	173.56	35.68	139.07	1.82
14	0.064	16.23	0.045	0.59	2.08	1.53	12.89	4.01	45.73	18.02	86.46	19.94	215.86	43.77	144.09	3
15	0.041	13.1	0.025	0.77	1.83	1.26	13.13	4.66	59.44	25.03	126.78	29.81	324.93	66.72	131.67	3.07
16	0.035	24.02	0.039	1.01	1.94	1.09	9.95	2.85	33.57	13.28	67.07	16.05	179.41	38.85	147.37	3.2
17	1.18	11.95	0.257	1.67	1.73	1.11	8.66	3.08	36.84	15.83	78.94	18.91	207.49	43.92	59.91	2.58
18	0.034	29.89	0.036	0.52	2.02	1.14	11.07	3.84	42.96	17.44	85.1	20.11	226.43	48.16	324.56	2.84

(*Continued*)

Table 4: Continued

Spots	La	Ce	Pr	Nd	Sm	Eu	Gd	Tb	Dy	Ho	Er	Tm	Yb	Lu	Y	Ti
	(ppm)															
19	0.038	10.48	0.037	0.52	1.52	1.08	9.46	3.16	39.26	16.07	79.93	18.73	202.94	42.98	131.77	2.23
20	0.05	19.48	0.029	0.4	2.12	1.19	11.85	3.97	47.93	19.71	97.75	22.91	245.93	50.86	262.5	2.21
SSYD01B2																
1	0.043	12.42	0.031	0.34	1.31	0.9	9.42	3.04	34.93	13.92	68.66	16.36	176.37	35.76	210.06	2.33
2	0.054	12.93	0.025	0.65	1.75	1.33	11.87	4.22	52.75	21.46	109.13	25.67	285.38	57.54	142.82	2.61
3	0.047	33.48	0.04	0.88	2.69	1.41	12.72	3.66	38.62	14.61	68.75	15.92	174.34	34.78	166.88	3.05
4	0.076	13.94	0.036	0.69	2.29	1.79	10.87	3.62	43.71	17.86	85.52	20.46	219.34	44.33	112.87	2.7
5	0.058	16.72	0.038	0.44	2.32	1.32	11.83	3.95	45.73	17.74	85.39	20.03	214.12	42.22	178.66	2.96
6	0.038	14.14	0.031	0.52	2.09	1.76	13.35	4.82	58.08	23.31	112.88	27.53	297	57.64	164	3.54
7	0.038	10.65	0.06	0.53	1.74	1.22	10.34	3.45	42.1	16.85	81.78	19.68	216.61	42.84	121.16	2.82
8	0.042	12.05	0.03	0.65	2.25	1.29	11.77	3.46	38.21	13.59	65.56	15.24	171.02	35.77	84.7	2.34
9	0.058	12.78	0.025	0.67	1.93	1.35	11.9	4.07	45.28	17.74	86.22	19.97	220.74	41.49	107.84	2.86
10	0.043	10.59	0.03	0.24	1.16	1	9.44	3.31	38.59	15.77	75.98	18.07	195.64	37.31	259.2	2.82
11	0.037	24.15	0.03	0.76	2.16	1.06	11.63	3.51	37.41	14.77	72.62	17.14	191.14	37.83	165.17	2.98
12	0.048	11.35	0.041	0.37	1.7	1.27	9.95	3.68	44.92	17.84	89.64	21.66	235.69	45.99	182.73	2.52
13	0.03	18.59	0.04	0.7	2.59	1.44	13.34	4.67	53.14	20.52	94.64	21.71	231.22	43.05	128.49	3.29
14	0.021	18.04	0.038	0.61	2.39	1.73	13.8	4.31	47.66	18.69	88.81	20.82	226.04	43.14	143.32	3.13
15	0.091	17.61	0.073	0.79	2.63	1.4	13.2	4.3	49.55	19.32	92.48	21.25	223.92	44.43	111.85	3.11
16	0.029	8.88	0.029	0.21	1.5	1.03	9.35	3.07	37.99	15.42	76.32	18.3	199.62	38.93	219.59	2.04
17	0.039	12.18	0.016	0.37	2.05	1.5	10.39	3.69	41.36	16.29	78.93	18.47	209.19	40.99	161.12	3.16
18	0.05	11.63	0.039	0.41	1.81	1.21	10.71	3.85	46.49	18.76	91.41	21.55	234.24	46.22	163.05	2.5
19	0.031	32.83	0.081	1	2.29	1.34	14.33	4.82	59.59	23.75	115.77	28.32	313.41	61.41	223.38	2.67
20	0.037	13.58	0.031	0.38	1.87	1.42	13.41	4.86	55.51	23.73	115.68	27.64	306.34	59.22	215.89	3.35
SSYD02B1																
1	0.044	9.59	0.038	0.66	1.29	1.08	9.54	3.57	43.64	18.48	92.7	22.37	252.49	51.13	121.77	2.59
2	0.036	14.7	0.039	0.59	1.99	1.5	13.3	5.03	59.3	23.99	117.2	27.57	300.78	58.21	158.83	3.2
3	0.064	13.42	0.024	0.47	1.86	1.29	11.8	3.82	45.15	17.59	85.14	20.23	216.11	42.67	154.08	2.86
4	0.035	13.89	0.024	0.36	2.26	1.47	12.8	5.08	60.89	24.8	120.96	28.83	315.79	62.98	216.86	3.34
5	0.04	14.03	0.02	0.31	2.05	1.33	11.15	4.03	48.08	18.55	90.97	21.7	233.09	46.17	224.5	3.21
6	0.05	8.88	0.036	0.54	1.72	1.15	12.33	4.7	60.78	26.54	133.49	33.01	366.93	75.3	133.34	4.5
7	0.077	12.76	0.057	0.47	1.11	0.92	9.27	2.83	35.39	13.62	72.56	18.28	211.77	43.07	208.11	3.47

(*Continued*)

Table 4: Continued

Spots	La	Ce	Pr	Nd	Sm	Eu	Gd	Tb	Dy	Ho	Er	Tm	Yb	Lu	Y	Ti
	(ppm)															
8	0.037	17.44	0.026	0.74	2.37	1.33	14.94	5.39	65.66	26.28	126.17	29.62	320.94	59.91	144.03	3.03
9	0.039	17.84	0.024	0.82	2.35	1.58	13.33	4.8	55.97	21.83	103.2	24.42	267.42	50.6	126.28	3.24
10	0.105	32.71	0.058	0.84	2.28	1.19	12.64	3.56	39.36	14.8	72.74	17.66	199.66	39.58	201.45	3.05
11	0.53	16.57	0.139	1.3	2.19	1.2	10.95	3.99	47.42	18.68	91.41	21.52	229.29	44.96	84.61	2.98
12	0.064	13.06	0.046	0.64	1.81	1.43	11.1	3.89	44.86	18.11	85.96	20.76	226.22	44.02	124.51	2.38
13	0.027	35.71	0.034	1	3.06	1.46	14.38	3.95	40.79	15.25	70.95	16.63	180.84	35	147.02	3.16
14	0.05	12.8	0.03	0.52	1.99	1.27	12.53	4.77	54.48	21.89	111.39	25.98	299.33	57.44	154.11	3.04
15	0.035	15.96	0.033	0.63	2.61	1.78	14.64	4.64	55.98	22.5	110.46	26.24	288.19	55.34	136.83	3.78
16	0.049	13.42	0.036	0.57	1.93	1.32	12.17	4.17	51.04	20.08	101.73	23.37	257.97	50.22	143.46	3.08
17	0.055	12.22	0.042	0.83	2.07	1.65	13.97	5.06	55.45	22.62	113.93	27.39	318.54	61.83	101.15	2.58
18	0.058	22.92	0.042	0.52	2.41	1.6	16.7	5.07	61.98	22.87	109.09	25.89	281.45	51.57	217.61	3.36
19	0.112	9.65	0.025	0.8	1.13	1.05	10.19	3.83	48.4	20.02	98.32	24.44	272.91	52.51	113.84	3.27
20	0.034	13.38	0.046	0.6	2.33	1.64	14.59	5.57	72.72	31.05	160.39	39.32	443.64	85.98	166.12	2.48

Table 5: Lu-Hf isotopic compositions of samples from the Tiezhai, Jinxingtou, and Sanshanyu complexes in the Luxi Terrane.

Spots	Ages (Ma)[1]	$^{176}Yb/^{177}Hf$	$^{176}Lu/^{177}Hf$	$^{176}Hf/^{177}Hf$	2σ	$\varepsilon_{Hf}(t)$	T_{DM} (Ma)	T_{DM}^{C} (Ma)	$f_{Lu/Hf}$
TZ16D03B2									
1	125	0.072652	0.001668	0.282795	0.000022	3	659	963	-0.95
2	125	0.118597	0.003054	0.282834	0.000040	4.3	626	882	-0.91
3	125	0.090907	0.002068	0.282832	0.000031	4.3	613	882	-0.94
4	125	0.279132	0.007413	0.282889	0.000124	5.8	621	782	-0.78
5	125	0.087712	0.002084	0.282910	0.000041	7	499	706	-0.94
6	125	0.115654	0.003587	0.282913	0.000053	7	516	707	-0.89
7	2512	0.032602	0.000776	0.281457	0.000023	8.8	2493	2483	-0.98
8	247.6	0.043865	0.000871	0.282726	0.000023	3.3	743	1043	-0.97
9	125	0.034709	0.003095	0.282868	0.000092	5.5	577	806	-0.91
10	125	0.108762	0.002218	0.282931	0.000032	7.8	470	658	-0.93
TZ16D04B2									
1	123	0.106222	0.002131	0.282904	0.000038	6.8	509	721	-0.94
2	123	0.157252	0.005431	0.282685	0.000064	-1.2	910	1231	-0.84
3	123	0.102010	0.002047	0.282854	0.000033	5	580	833	-0.94
4	123	0.341220	0.009373	0.282790	0.000114	2.1	843	1016	-0.72
5	301	0.147682	0.002937	0.283119	0.000042	18	197	143	-0.91
6	123	0.105434	0.001972	0.282893	0.000024	6.4	523	745	-0.94
7	123	0.073933	0.001477	0.282802	0.000026	3.2	646	948	-0.96
8	123	0.094377	0.001885	0.282747	0.000032	1.2	733	1075	-0.94
9	123	0.263562	0.007398	0.282701	0.000069	-0.9	941	1206	-0.78
10	123	0.069743	0.001419	0.282773	0.000031	2.2	687	1014	-0.96
TZ16D07B1									
1	123	0.015357	0.000352	0.282687	0.000023	-0.8	787	1203	-0.99
2	123	0.013346	0.000310	0.282704	0.000020	-0.2	762	1164	-0.99
3	123	0.032492	0.000674	0.281989	0.000051	-26	1761	2763	-0.98
4	123	0.036620	0.000813	0.282810	0.000016	3.6	623	927	-0.98
5	123	0.020400	0.000450	0.282678	0.000026	-1.1	801	1223	-0.99
6	123	0.021276	0.000486	0.282633	0.000022	-2.7	865	1326	-0.99
7	123	0.038046	0.000836	0.281986	0.000018	-26	1772	2771	-0.97
8	123	0.024856	0.000519	0.282735	0.000038	0.9	723	1094	-0.98
9	203	0.020267	0.000463	0.282657	0.000022	-0.1	831	1220	-0.99
10	123	0.021485	0.000495	0.282696	0.000015	-0.5	778	1183	-0.99
JX16D02B1									
1	122	0.051045	0.000993	0.282475	0.000038	-8.3	1098	1682	-0.97
2	2539	0.020265	0.000428	0.281304	0.000018	4.6	2676	2762	-0.99
3	2539	0.017748	0.000372	0.281287	0.000019	4.1	2695	2793	-0.99
4	2539	0.014129	0.000338	0.281277	0.000017	3.8	2707	2813	-0.99
5	2539	0.018096	0.000356	0.281264	0.000014	3.3	2726	2843	-0.99
6	2539	0.012273	0.000262	0.281294	0.000020	4.5	2679	2766	-0.99
7	122	0.015667	0.000347	0.282451	0.000020	-9.1	1113	1733	-0.99
8	2539	0.020978	0.000462	0.281247	0.000018	2.5	2756	2891	-0.99
9	122	0.039370	0.000804	0.282494	0.000020	-7.6	1066	1639	-0.98
10	122	0.011390	0.000960	0.282479	0.000119	-8.2	1092	1674	-0.97

(*Continued*)

Table 5: Continued

Spots	Ages (Ma)[1]	$^{176}Yb/^{177}Hf$	$^{176}Lu/^{177}Hf$	$^{176}Hf/^{177}Hf$	2σ	$\varepsilon_{Hf}(t)$	T_{DM} (Ma)	T_{DM}^{C} (Ma)	$f_{Lu/Hf}$
JX16D03B1									
1	120	0.066351	0.001166	0.282597	0.000252	-4.1	932	1411	-0.96
2	120	0.036303	0.000908	0.282606	0.000105	-3.7	913	1390	-0.97
3	120	0.078015	0.001398	0.282763	0.000065	1.8	700	1037	-0.96
4	120	0.045640	0.000906	0.282598	0.000043	-4	924	1408	-0.97
5	120	0.062495	0.001437	0.282740	0.000026	1	734	1090	-0.96
6	120	0.026911	0.000507	0.282602	0.000362	-3.9	909	1397	-0.98
7	120	0.036690	0.000808	0.282606	0.000021	-3.7	909	1388	-0.98
8	2505	0.016868	0.000370	0.281290	0.000024	3.4	2692	2809	-0.99
9	120	0.059254	0.001313	0.282715	0.000027	0.1	767	1145	-0.96
10	120	0.028714	0.000545	0.282800	0.000367	3.1	633	950	-0.98
SSY16D01B1									
1	125	0.054035	0.001107	0.282677	0.000020	-1.1	817	1228	-0.97
2	125	0.015981	0.000347	0.282678	0.000019	-1	799	1221	-0.99
3	125	0.034463	0.000757	0.282627	0.000021	-2.9	879	1339	-0.98
4	125	0.038729	0.000805	0.282659	0.000018	-1.8	836	1267	-0.98
5	125	0.033168	0.000736	0.282643	0.000022	-2.3	856	1302	-0.98
6	125	0.046165	0.000964	0.282625	0.000019	-3	887	1343	-0.97
7	125	0.047487	0.001264	0.282639	0.000021	-2.5	873	1313	-0.96
8	125	0.035729	0.000918	0.282629	0.000018	-2.8	880	1335	-0.97
9	125	0.023859	0.000517	0.282629	0.000017	-2.8	870	1332	-0.98
10	125	0.021412	0.000448	0.282723	0.000020	0.5	739	1121	-0.99
SSY16D01B2									
1	123	0.039803	0.000841	0.282630	0.000020	-2.8	876	1332	-0.97
2	123	0.040748	0.000921	0.282703	0.000021	-0.2	776	1168	-0.97
3	123	0.053411	0.000988	0.282722	0.000027	0.4	750	1126	-0.97
4	123	0.028395	0.000658	0.282693	0.000020	-0.6	785	1190	-0.98
5	123	0.017278	0.000389	0.282714	0.000020	0.2	750	1142	-0.99
6	123	0.039797	0.000845	0.282644	0.000019	-2.3	858	1302	-0.97
7	123	0.044581	0.000995	0.282562	0.000029	-5.2	976	1487	-0.97
8	123	0.025074	0.000555	0.282706	0.000013	-0.1	765	1161	-0.98
9	123	0.017362	0.000389	0.282570	0.000016	-4.9	949	1465	-0.99
10	123	0.022783	0.000502	0.282757	0.000024	1.7	692	1045	-0.98
SSY16D02B1									
1	123	0.036139	0.000752	0.282616	0.000019	-3.3	895	1364	-0.98
2	123	0.041579	0.001114	0.282620	0.000053	-3.2	898	1358	-0.97
3	123	0.040736	0.000853	0.282671	0.000017	-1.4	819	1240	-0.97
4	123	0.034399	0.000752	0.282676	0.000018	-1.2	811	1230	-0.98
5	123	0.032626	0.000694	0.282629	0.000019	-2.9	876	1336	-0.98
6	123	0.019681	0.000584	0.282644	0.000034	-2.3	851	1300	-0.98
7	123	0.040946	0.000853	0.282615	0.000017	-3.4	899	1368	-0.97
8	123	0.006591	0.000551	0.282574	0.000053	-4.8	949	1458	-0.98
9	123	0.038720	0.000850	0.282623	0.000014	-3.1	887	1348	-0.97

(*Continued*)

TABLE 5: Continued

Spots	Ages (Ma)[1]	$^{176}Yb/^{177}Hf$	$^{176}Lu/^{177}Hf$	$^{176}Hf/^{177}Hf$	2σ	$\varepsilon_{Hf}(t)$	T_{DM} (Ma)	T_{DM}^{C} (Ma)	$f_{Lu/Hf}$
10	123	0.044048	0.000934	0.282673	0.000017	-1.3	818	1236	-0.97

[1]Calculated age for $\varepsilon_{Hf}(t)$ values.

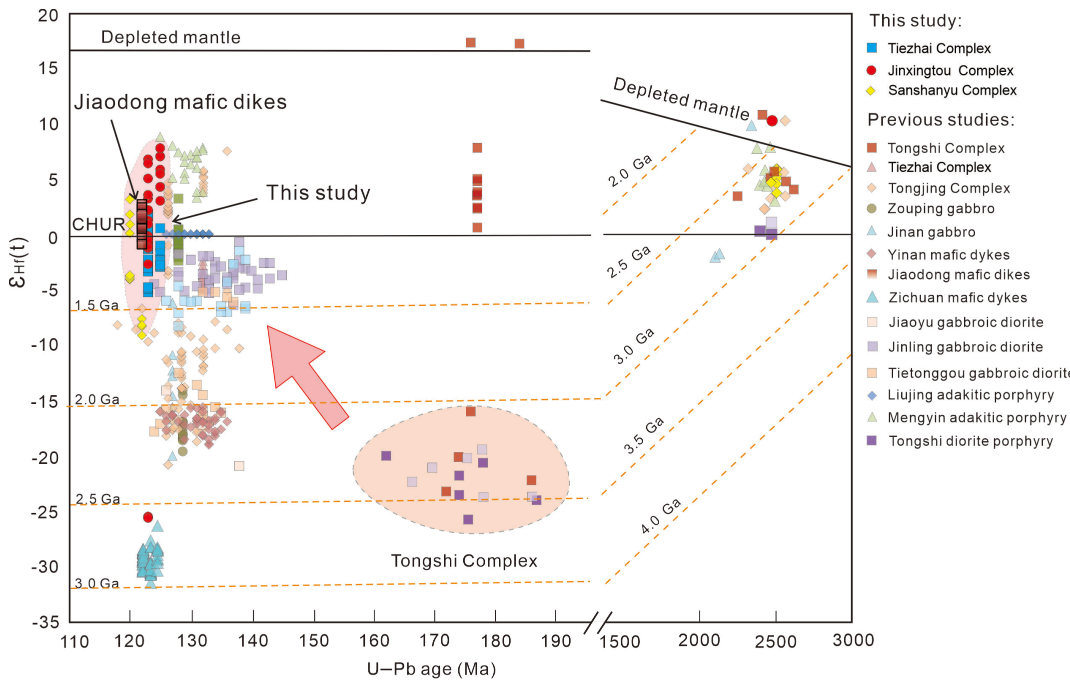

FIGURE 8: Zircon ε_{Hf} (t_1) values versus U-Pb ages from the igneous rocks. Data sources: Tiezhai Complex (References 8, 52; this study); Liujing and Mengyin porphyries [6]; Tietonggou Complex [50]; Zichuan mafic dykes [17]; Jinling, Zouping and Jinan mafic dykes [48, 51]; Tongshi and Tongjing complexes [3, 57]; Yinan Complex [48]; Jiaodong diabase porphyry [34]; Sanshanyu and Jinxingtou complexes (this study).

magmas [73]. In the MgO, Th/Ce and Yb versus SiO_2 plots, most samples fall in the field of the delaminated lower crust-derived adakitic rocks, indicating that adakitic magma passed through the lithospheric mantle and react with mantle peridotite as they rise (Figures 10(a)–10(d); [74]). In addition, the high Sr/Y and La/Yb concentrations for residual melts could be mainly controlled by magma mixing rather than fractional crystallization, evidenced by no obvious correlation between the Sr/Y, La/Yb ratios, and SiO_2 in the adakitic samples in the Luxi Terrane (Figures 11(a) and 11(b); [4]). The Nb/Ta ratios of "High Sr/Y granitoids" (14.68, 28.29, average value = 17.62) are obviously higher than the average value of lower crust (8.3) [64], also ruling out the possibility of thickened mafic lower crust source. In addition, geochemical modeling reveals that these samples also display magma mixing trends in the Th versus Th/V and 1 /V versus Sm/V diagrams, where Th and Sm act as C^I elements and V acts as a C^C element (Figures 11(c) and 11(d)).

(4) Isotopic evidence. In this study, the ε_{Hf} (t_1) values of the syenites can be divided into two groups: (−25.5 to −25.6) with T_{DM}^{C} ages = (2.76, 2.77 Ga) and (−4.9, 3.6) with T_{DM}^{C} ages = (927, 1487 Ma). A huge variation of Hf isotope indicates the involvement of the magma derived from the reworking of the ancient basement. In addition, the wide range of ε_{Hf} (t_1) values (from −31.4 to +7.8) of the Early Cretaceous adakites in the Luxi Terrane is intermediate between those of completely mantle-derived lamproites (from −0.9 to +2.7) and Jurassic diorites in Tongshi Complex (−27, −16), further supporting a hybrid origin (Figure 8).

To sum up, we propose that the "High Sr/Y Granitoids" in Luxi Terrane were formed by magma mixing of mafic and felsic melts. In addition, previous studies believed that the high Sr/Y geochemical characteristics can be interpreted by: (1) the presence of garnet as a residual or fractionating phase [15, 75] or (2) plagioclase + amphibole + clinopyroxene accumulation and interstitial melt loss in "crystal

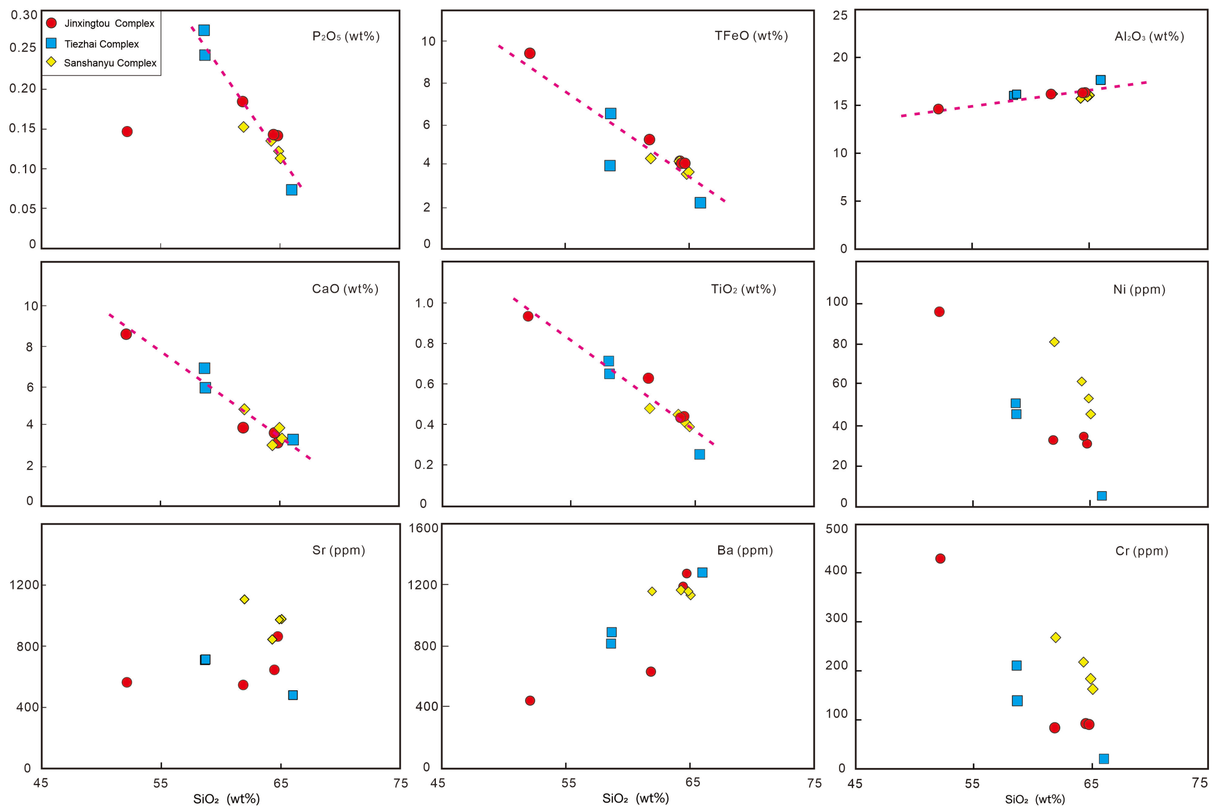

FIGURE 9: Elemental variation diagrams showing possible fractionating phases during magma evolution.

mush model" [76]. The blue field in which some "High Sr/Y Granitoids" fell can be interpreted to reflect varying degrees of plagioclase + amphibole + clinopyroxene accumulation [76]. Meanwhile, the high Sr/Y rocks also plot between the partial melting curves for garnet amphibolite and amphibolite restites (Figures 10(e) and 10(f)). Therefore, both the two fractionation crystallization processes may exist in the magma emplacement, but magma mixing still dominates. Thus, it is difficult to further discuss fractional crystallization under the background of the magma mixing process.

5.1.2. Source Characteristics of Mafic and Felsic End-Members. Macroscale evidence leads us to support that the High Sr/Y granitoids were predominantly generated by magma mixing between relatively mafic magma and felsic melts. Melting of such a magma source would yield a melt in which the major elements are dominated by mantle components, while the trace elements and isotopic compositions are governed by the crustal components [4]. Therefore, we present the following discussions about the characteristics of mafic and felsic end-members.

The mafic intrusions (SiO_2 < 53%) such as gabbroic diorites and gabbro have widely $\varepsilon_{Hf}(t_1)$ (−31.4, 0; Figure 8) and $Mg^{\#}$ (up to 50) values, pointing out the incorporation of metasomatized-mantle mafic melts. The high La/Nb and Ba/Nb ratios of the "High Sr/Y granitoids" also fall into the field of the arc volcanics (Figure 5(b)), implicating that the mantle source of the Luxi Terrane was similar to the mantle wedge in the subduction zone [46]. In addition, the high LILEs could be inherited from basic magmas derived from a lithospheric mantle that previously metasomatized by subduction zone fluids/melts (Figure 11(e); [7, 23]).

Physical conditions (e.g., temperature and H_2O content) can also control the composition of magma by influencing the magmatic process [77]. The mixing process between two magma end-members indicates that the viscosity of the mafic magmas was not significantly different from that of the felsic end-members [78]. Because melt viscosity is highly dependent on water content and temperature [79], the mafic end-members involved in magma mixing should be water-rich and therefore rather evolved. In addition, the contribution from such a metasomatized mantle is also manifested by the abundance of euhedral hornblende in these high Sr/Y rocks, which indicates an H_2O-rich parental magma (Figures 4(c), 4(e), and 4(f)). The oxygen fugacity and crystallization temperature of magma were estimated by the Ce anomaly and Ti thermometer, respectively. The results showed that the magma had a high-oxygen fugacity that ranges between FMQ and MH (ΔFMQ [fO_2] = 0.62–4.02; T = 636°C–776°C; Table 6). They show Ti-in-zircon temperatures ranging from 636°C to 676°C, which are much lower than those of amphibole-dehydration melting reactions (850°C–900°C [80]) but similar to those of water-fluxed melting reactions under crustal pressures (<800°C; [77]).

These mantle-related magmas with significantly elevated MgO (>3 wt%), Cr, and Ni concentrations and high $Mg^{\#}$ values (>50 [36]) were formed by the partial melting of the delaminated lower continental crust in the mantle produces adakitic magma that ascends and interacts with overlying

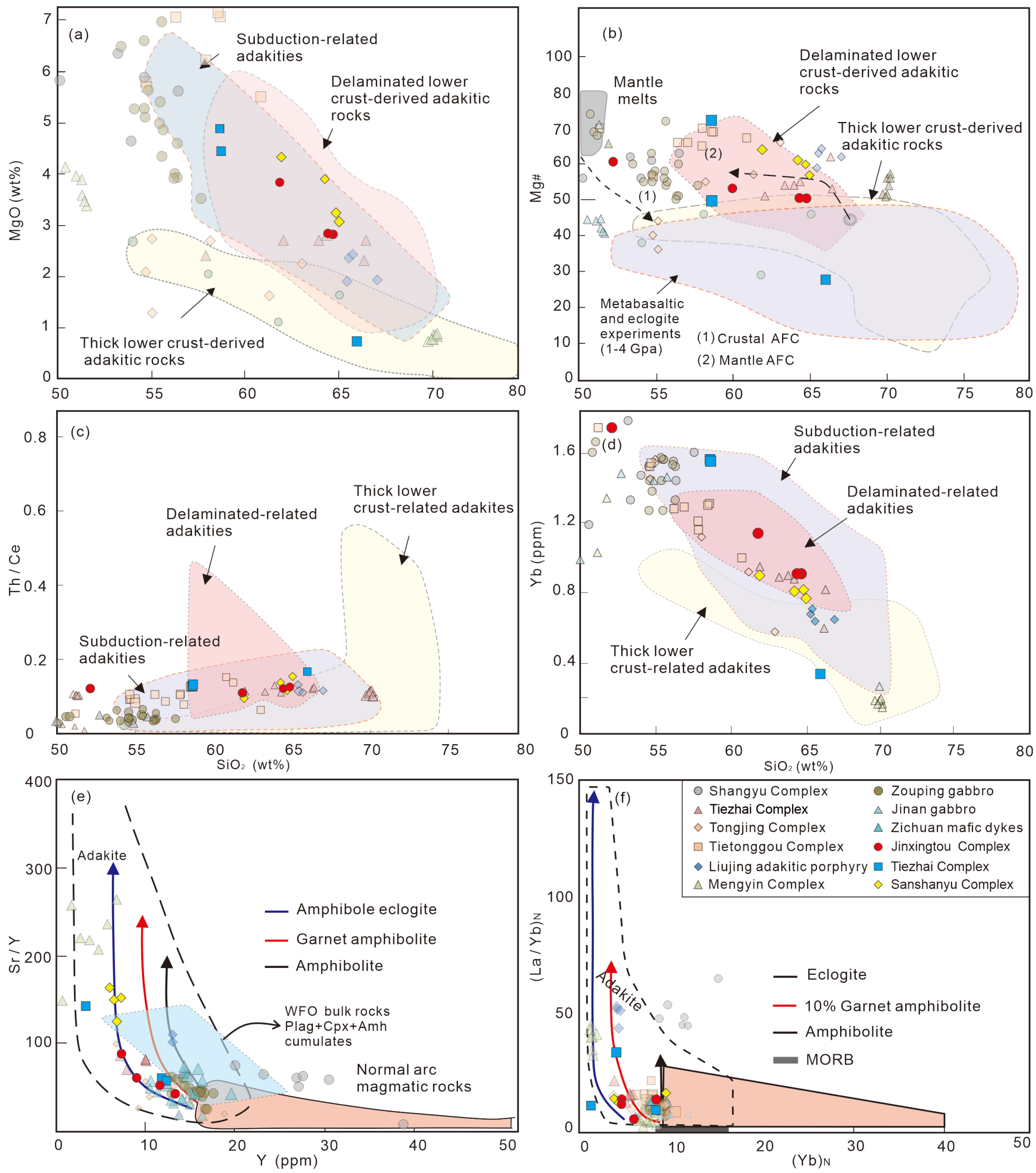

Figure 10: (a) Mg versus SiO_2 diagram. (b) Mg# versus SiO_2 diagram (after References 101, 102). (c) Th/Ce versus SiO_2 diagram. (d)Yb versus SiO_2 diagram. Fields of metabasaltic and eclogitic experimental melts, delaminated and thick lower crust-derived adakitic rocks are after Reference 101. Source (1) is a supposed pure slab melt [74], and source (2) is the metabasaltic or eclogitic experimental melt which is not hybridized by mantle peridotite [81]. (e) Sr/Y versus Y [1]. (f) $(La/Yb)_N$ versus Yb_N diagram [103], curves show calculated partial melting trends. The blue field overlapping Western Fiordland Orthogness (WFO) bulk rocks is interpreted to reflect varying degrees of plagioclase + amphibole + clinopyroxene accumulation [76]. Data sources: Data sources of the high-Mg adakites in the Luxi Terrane: Tiezhai Complex ([20]; this study); Shangyu Complex [54]; Liujing and Mengyin porphyries [6]; Tietonggou Complex [50]; Zouping and Jinan mafic dykes [51]; Mengyin and Zichuan mafic dykes [11]; Tongjing Complex [49]; Sanshanyu and Jinxingtou complexes (this study).

mantle peridotite material. These chemical characteristics are similar to the results of experiments involving the interaction with melts and peridotite [81] and can be attributed to the mantle-derived high-Mg basic magma, compounded by the entrainment of pyroxene (and olivine) xenocryst [4, 14]. We therefore suggest that the gabbroic diorite (Sample JX1601B1, SiO_2 = 52.1%, Mg# = 62) is the best candidate that reflects the most primitive adakite magmas of the mantle-derived source.

The samples in this study display a slight evolution trend from calc-alkaline to high-K calc-alkaline series (Figure 6(b)), indicating the increasing incorporation of potassium-rich crustal compositions. All of the diorites, syenites, and monzogranites are peraluminous rocks (A/CNK = 1.1–1.4; Figures 6(b) and 6(c)), also suggesting the involvement of evolved, high-K crust-derived melts. Based on the magma mixing model proposed by Chen et al. [4], felsic melts could be formed as a result of the underplating of

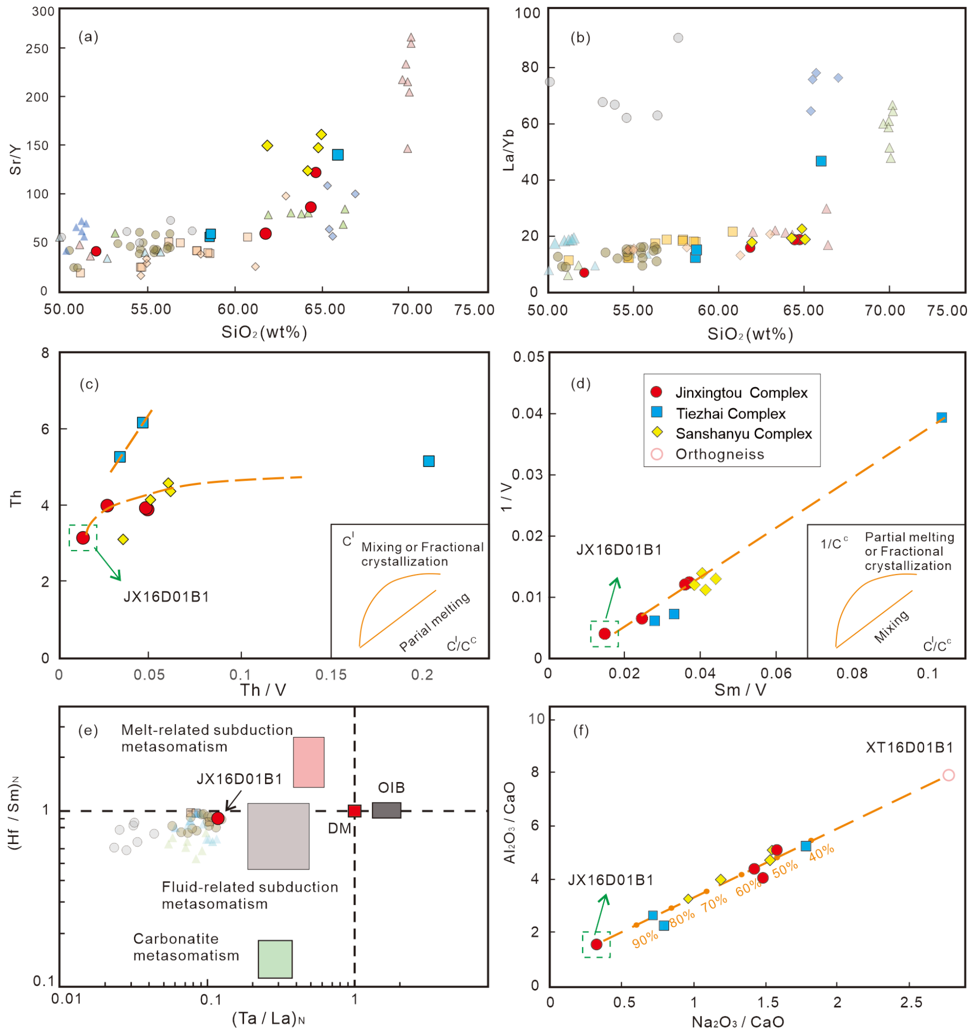

FIGURE 11: Petrogenetic discrimination and magma mixing modeling diagrams for the adakitic porphyry samples. (a) Sr/Y versus SiO_2 diagram. (b) La/Yb versus SiO_2 diagram. (c) Th (ppm) versus Th/V diagram showing that the geochemical variations in the samples from the Luxi Terrane are dominantly controlled by magma mixing. The inset is a schematic C^I versus C^I/C^C plot, where the superscripts I and C are incompatible and compatible elements, respectively. (d) 1 /V versus Sm/V diagram. The inset is a schematic $1/C^I$ versus C^I/C^C plot. (e) $(Hf/Sm)_N$ versus $(Ta/La)_N$ diagrams for mafic dykes in the NCC [82]. (f) Al_2O_3/CaO versus Na_2O/CaO diagram.

basic magma in the lower crust, which triggered partial melting of the basement rocks (Archean mafic granulites and TTG gneisses). In addition, the occurrence of Neoarchean–Paleoproterozoic inherited zircons indicates that the ancient lower crust in the NCC participated in the formation of the magma process during magma ascent [46, 50, 51, 82]. To reveal the interaction between ancient crustal basements and Mesozoic magma events in the Luxi Terrane, we plot the recently published inherited data of the intrusions in the ε_{Hf} (t_2) versus age data (Figure 8). The inherited zircons have a $^{207}Pb/^{206}Pb$ age range between 2.51 and 2.35 Ga (concentrate on ca. 2.5 Ga), positive ε_{Hf} (t_2) values (2.5, 8.8), and $T_{DM}{}^C$ values (2.6, 2.8 Ga). The U-Pb ages and the ε_{Hf} (t_1) values of the inherited zircons from the Early Cretaceous intrusive rocks in the Luxi Terrane are consistent with the formation of ancient basement rocks (2.65, 2.50 Ga) [39, 40, 54, 83, 84]. The Neoarchean inherited zircons were related to the most large-scale crustal accretion and reactivation in the NCC [24, 30, 85]. The widely distributed Late Archean-Early Paleoproterozoic TTGs (2.57, 2.30 Ga) in the southern NCC consist of both juvenile and reworked materials, which are mostly attributed to the accretionary orogen accompanied by the basaltic underplating [51, 85]. The observation of dominantly juvenile lower crust in the southern NCC during the Late Archean to Early Paleoproterozoic is consistent with positive ε_{Hf} (t_2) values in most inherited zircons. TTGs constituted dominant components of the Precambrian continental crust of the NCC [39]. Thus, we propose the orthogneiss sample collected in the Luxi Terrane (XT16D01B1, SiO_2 = 60.94%, $Mg^\#$ = 37 [40]) can be taken as a presumed felsic end-member candidate.

Based on the hypothetical mafic and felsic end-members as mentioned above, we process classic major elements two end-members mixing model following the equation of $C_m = C_{a\ (1-x)} + C_{b\ x}$ [86], the C_m represents the contents of

Table 6: Crystallization temperature and zircon oxygen fugacity of samples from the Tiezhai, Jinxingtou, and Sanshanyu complexes in the Luxi Terrane.

No.	Samples	δCe[1]	t^{Mean}(°C)[2]	Lg(fO_2)[3]	ΔFMQ[4, 5]
1	JX16D02B1	96	719.0	−12.33	4.02
2	JX16D03B1	105.5	666.0	−14.94	2.8
3	TZ16D03B2	49.6	776.1	−11.96	3.05
4	TZ16D04B2	36.5	727.6	−15.51	0.62
5	TZ16D07B1	79.05	704.5	−13.84	2.87
6	SSY16D01B1	162	636.5	−15.13	3.46
7	SSY16D01B2	163	640.7	−14.84	3.62
8	SSY16D02B1	153	647.6	−14.65	3.61

[1] $\left(\frac{Ce}{Ce*}\right)_D \approx \left(\left(\frac{Ce}{Ce*}\right)\right)_{CHUR} = \frac{CeN}{\sqrt{LaN*PrN}}$.

[2] Log (ppm Ti-in-zircon) = $(5.711 \pm 0.072) - \frac{(4800 \pm 86)}{T(K)} - \log\alpha SiO2 - \log \alpha TiO2$ [104].

[3] In $\left(\frac{Ce}{Ce*}\right)_D = (0.1156 \pm 0.0050) * \text{In}\ (fO_2) + \frac{13860 \pm 708}{T(K)} - 6.125 \pm 0.484$ [105].

[4] FMQ log $(fO_2) = \frac{-24441.9}{T(K)} + (8.290 \pm 0.167)$ [106].

[5] $\Delta FMQ = \log (fO_2) - FMQ$.

hybrid magma, and C_a and C_b represent the compositions of felsic and mafic end-members, respectively. The x is the mass fraction of the felsic end-member. In this study, the composition of the metasomatized mantle-derived gabbroic diorite was used as mantle-derived mafic end-member and the ancient crust-derived TTG gneiss as felsic end-member. The major element contents of the gabbroic diorite, monzogranites, diorites, and syenites plot on a straight line that passes through the origin (Figure 11(f)), suggesting that the "High Sr/Y granitoids" can be produced by the magma mixing of felsic melts and relatively mafic melts. The syenite and monzonite are more evolved than diorites. The results indicate that the High Sr/Y granitoids were derived from the magmatic precursors of gabbroic diorite with the addition of (10%–60%) ancient lower crust in the Luxi Terrane. Combining the above lines of evidence derived from petrological, petrographical, and geochemical data, we conclude that the magmatic precursors of these High Sr/Y granitoids were dominantly derived from magma mixing [87].

5.2. Geodynamic Implications. As demonstrated above from field and geochemical evidence, these intermediate-acid high-Mg adakites of the Luxi Terrane may not represent adakitic primitive magma. In contrast, they are suggested to generate from a mixture of a metasomatized mantle-derived basic magma and a crustal melt, followed by limited fractionation of ferromagnesian phases and entrainment of xenolitic crystals [4]. In addition, the formation of high-Mg adakite from different sources in the Luxi Terrane has demonstrated that the involvement of subduction-related materials and crustal recycling became dominant during late Mesozoic magmatism in the NCC (Figure 6(d); [4, 6, 11]). The eclogite was likely to delaminate and be recycled into the mantle due to its higher density and lower melting temperature than lithospheric mantle peridotite in the Early Cretaceous [19, 81]. Meanwhile, depleted mantle material also participated in the formation of the Early Cretaceous magma in a dynamic process [3]. The ε_{Hf} (t_1) values of the intrusive rocks in the Luxi Terrane show a systematic change from highly negative to nearly positive, indicating that the upwelling of the asthenosphere under the strongly thinned subcontinental lithosphere from 130 to 120 Ma [6, 46, 47].

Numerous mafic dykes were emplaced in the NCC during Mesozoic suggesting an extensional tectonic regime during the Early Cretaceous [33, 42]. Lithospheric extension beneath NCC has also been supported by several lines of evidence, including a series of fault basins, widespread metamorphic core complexes, and associated voluminous magmatism [23, 46, 82]. The large-scale extension and voluminous magmatism resulted in extensive destruction of the NCC [19, 42]. Recent geological and geophysical studies have shown that the slab rollback of the Paleo-Pacific slab beneath the eastern NCC caused the extension of the lithospheric mantle and upwelling of the asthenosphere during the late Mesozoic [12, 21, 32, 42, 46, 88]. The destruction of the NCC can also be first-order linked with the evolution of the Paleo-Pacific subduction [89]. By matching the subduction stage of the Paleo Pacific plate with the formation process of the Early Cretaceous high Mg adakite rocks in the studied area, we can clearly describe the process of crust-mantle interaction beneath the Luxi Terrane [6, 23].

At ca. 185–175 Ma, the subduction of the Paleo-Pacific plate led to a few magmatic activities in the Luxi Terrane, such as the emplacement of the Tongshi Complex [23, 35, 47]. The enriched mantle has not yet melted completely, and some asthenosphere material has been added to the magma source in the Middle Jurassic, evidenced by the zircon $\varepsilon_{Hf}(t)$ values (−25, −10) of the intrusive rocks (Figure 12(a); [47, 57, 66]). At ca. 144 Ma, the subducted Paleo-Pacific slab rolled back, causing continental arc-rifting and the lithosphere bottom to be heated by the upwelling asthenospheric mantle (Figure 12(b); [90, 91]). And the basaltic magmas also underplated the lower crust to form the newly thick amphibole-bearing eclogite lower crust [35]. Until ca. 135 Ma, the progressive slab rollback caused the founder of the newly underplated thick lower crust within the shallow lithospheric mantle. The gabbroic diorite (sample JX16D01B1) discussed in this section was supposed to be derived from the partial melting of delaminated newly underplated thick lower crust that interacted with above asthenospheric mantle peridotite [6]. The underplating of the hot mantle-derived mafic magmas beneath the crust further triggered the reworking of the Neoarchean basement of the NCC, forming the felsic end-member (Figure 12(c); [36]). Consequent magma mixing and AFC process might have resulted in the various lithologies and compositions of other rocks in the Luxi Terrane (see above discussions), including the "High Sr/Y granitoids."

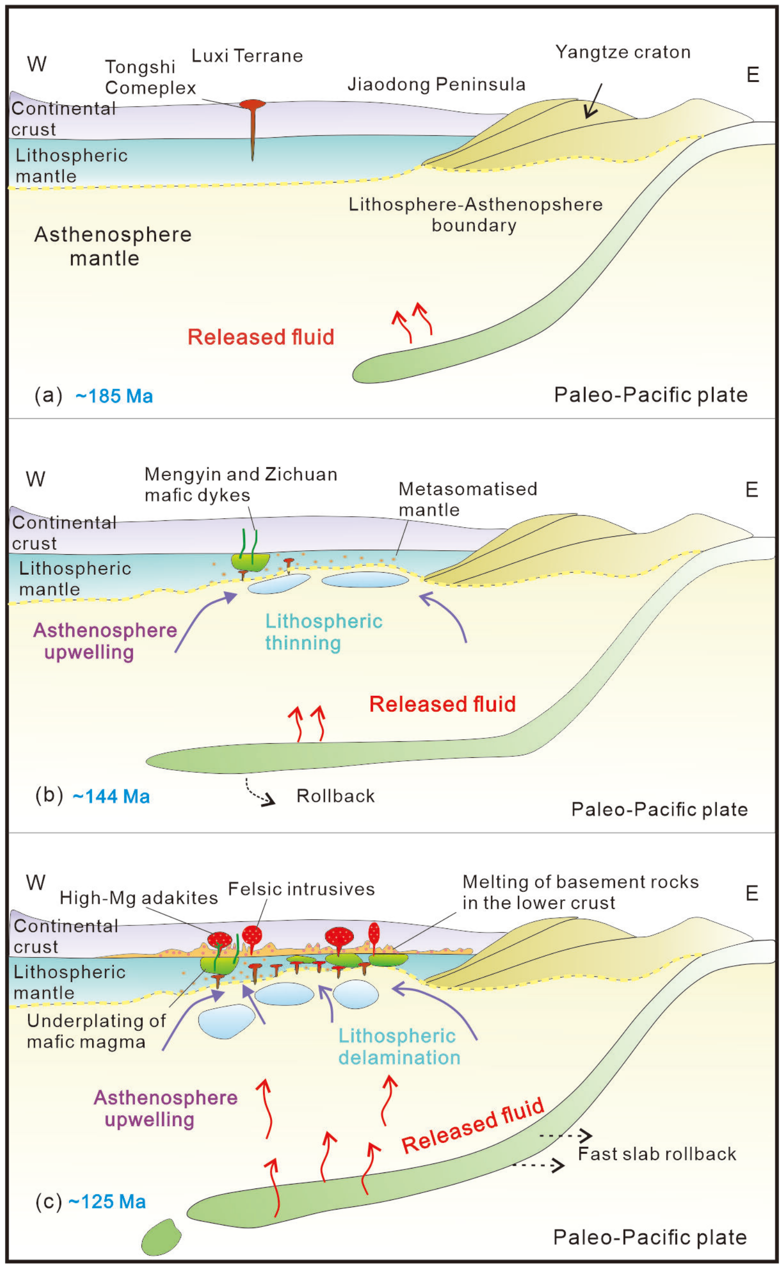

Figure 12: Schematic plate tectonic model showing lithospheric destruction of the North China Craton through thermal-chemical-mechanical erosion and lithospheric delamination (modified after Reference 82).

6. Conclusions

(1) The zircon U-Pb dating results indicate that the Tiezhai, Jinxingtou, and Sanshanyu adakitic magma intruded into the Luxi Terrane at 125–120 Ma. The Jinxingtou and Tiezhai adakitic rocks contain abundant Neoarchean–Paleoproterozoic inherited zircon cores with ages of 2.55–2.35 Ga. The three complexes were emplaced in the peak period of magmatic flare-up during the Early Cretaceous.

(2) The "high Sr/Y granitoids" of the three complexes were generated by magma mixing between metasomatized mantle-derived mafic melts and ancient crust-derived felsic melts. The mafic components of the adakitic rocks were derived from the delaminated lower crust and then interacted with the mantle peridotite. The felsic magma chambers were intruded by mantle-derived mafic magma resulting in varying degrees of magma mixing and mingling.

(3) In conjunction with regional geodynamic setting and published Hf isotopes of Mesozoic igneous rocks, we propose that the enriched mantle was gradually replaced by the depleted mantle during the intense crust-mantle interaction. The subduction processes of the Paleo-Pacific plate provided

significant chemical materials (e.g., the melts and fluids of the slab) and suitable environments (e.g., the extensional tectonic settings and upwelling flow) for the intense crust-mantle interaction in the NCC.

Data Availability

The data for this study are available in this manuscript and supplementary material.

Conflicts of Interest

The authors declare that they have no conflicts of interest.

Acknowledgments

This work was supported by National Key Research and Development Project of China (Number 2020YFA0714802), the National Natural Science Foundation of China (Numbers 41872080 and 92162101), and Most Special Fund from the State Key Laboratory of Geological Processes and Mineral Resources in China University of Geosciences (Beijing) of China (Number MSFGPMR201804). We thank the team members from China University of Geosciences (Beijing) for their support in the field. We are also grateful to the anonymous referees for their helpful comments.

References

[1] M. J. Defant and M. S. Drummond, "Derivation of some modern arc Magmas by melting of young Subducted Lithosphere," *Nature*, vol. 347, no. 6294, pp. 662–665, 1990.

[2] P. R. Castillo, "Adakite Petrogenesis," *Lithos*, vols. 134–135, March, pp. 304–316, 2012.

[3] Y. G. Xu, X. Y. Wu, Z. Y. Luo, J. L. Ma, X. L. Huang, and L. W. Xie, "Zircon HF Isotope compositions of middle Jurassic-early Cretaceous intrusions in Shandong province and its implications," *Acta Petrologica Sinica*, vol. 23, no. 2, pp. 307–316, 2007.

[4] B. Chen, B. M. Jahn, and K. Suzuki, "Petrological and nd-SR-os isotopic constraints on the origin of high-mg Adakitic rocks from the North China Craton," *Geology*, vol. 41, no. 1, pp. 91–94, 2013.

[5] W. L. Xu, Q. J. Zhou, F. P. Pei, et al., "Destruction of the North China Craton: Delamination or thermal/chemical erosion? Mineral chemistry and oxygen isotope insights from websterite xenoliths," Gondwana Research, vol. 23, pp. 119–129, 2013.

[6] H. Wang, Z. Xu, X. Lu, et al., "Two-types of the early Cretaceous Adakitic Porphyries from the Luxi Terrane, Eastern North China block: Melting of Subducted paleo-Pacific slab and Delaminated newly Underplated lower crust," *Lithos*, vols. 240–243, January, pp. 140–154, 2016.

[7] C. Zhang, C. Q. Ma, F. Holtz, J. Koepke, P. E. Wolff, and J. Berndt, "Mineralogical and Geochemical constraints on contribution of Magma mixing and fractional crystallization to high-mg Adakite-like Diorites in Eastern Dabie Orogen, East China," *Lithos*, vols. 172–173, July, pp. 118–138, 2013.

[8] X. H. Sun, H. S. Tang, and Y. Luan, "Petrogenesis and Tectonic implications of the early Cretaceous Dagushan Adakitic Porphyries in the Anshan area, North China Craton," *Acta Geochimica*, vol. 41, no. 1, pp. 24–38, 2022.

[9] P. R. Castillo, P. E. Janney, and R. U. Solidum, "Solidum, Petrology and geochemistry of Camiguin Island, Southern Philippines: Insights to the source of Adakites and other Lavas in a complex arc setting," *Contributions to Mineralogy and Petrology*, vol. 134, no. 1, pp. 33–51, 1999.

[10] M. J. Streck, W. P. Leeman, and J. Chesley, "High-Magnesian Andesite from mount Shasta: a product of Magma mixing and contamination, not a primitive Mantle melt," *Geology*, vol. 35, no. 4, p. 351, 2007.

[11] S. Liu, R. Hu, S. Gao, et al., "Zircon U–PB Geochronology and major, trace elemental and SR–nd–PB isotopic geochemistry of Mafic Dykes in Western Shandong province, East China: Constrains on their Petrogenesis and Geodynamic significance," *Chemical Geology*, vol. 255, nos. 3–4, pp. 329–345, 2008.

[12] L. H. Chen and X. H. Zhou, "Subduction-related Metasomatism in the thinning Lithosphere: Evidence from a composite Dunite-Orthopyroxenite Xenolith Entrained in Mesozoic Laiwu high-mg Diorite, North China Craton," *Geochemistry, Geophysics, Geosystems*, vol. 6, no. 6, pp. 1–20, 2005.

[13] H.-O. Gu, Y. Xiao, M. Santosh, et al., "Spatial and temporal distribution of Mesozoic Adakitic rocks along the tan-LU fault, Eastern China: Constraints on the initiation of Lithospheric thinning," *Lithos*, vol. 177, September, pp. 352–365, 2013.

[14] W. L. Xu, S. Gao, Q. H. Wang, D. Y. Wang, and Y. S. Liu, "Mesozoic Crustal thickening of the Eastern North China Craton: Evidence from Eclogite Xenoliths and Petrologic implications," *Geology*, vol. 34, no. 9, 2006.

[15] J. F. Moyen, "High SR/Y and La/Yb ratios: The meaning of the "Adakitic signature," *Lithos*, vol. 112, nos. 3–4, pp. 556–574, 2009.

[16] N. Petford and M. Atherton, "Na-rich partial melts from newly Underplated Basaltic crust: The Cordillera Blanca Batholith, Peru," *Journal of Petrology*, vol. 37, no. 6, pp. 1491–1521, 1996.

[17] S. Liu, C. X. Feng, M. G. Zhai, et al, "Zircon U-PB age, Geochemical, and SR-nd-HF isotopic constraints on the origin of early Cretaceous Mafic Dykes from Western Shandong province, Eastern North China Craton, China," *Acta Petrologica Sinica*, vol. 32, no. 3, pp. 629–645, 2016.

[18] J. F. Xu, S. Ryuichi, J. Marc, Q. Wang, and R. P. Rap, "Origin of Mesozoic Adakitic intrusive rocks in the Ningzhen area of East China: Partial melting of Delaminated lower Continental crust?," *Geology*, vol. 30, no. 12, pp. 1111–1114, 2002.

[19] S. Gao, R. L. Rudnick, H.-L. Yuan, et al., "Recycling lower Continental crust in the North China Craton," *Nature*, vol. 432, no. 7019, pp. 892–897, 2004.

[20] L. D. Yu, X. F. Yu, D. P. Li, et al, "Zircon U-PB chronology, geochemistry characteristics of the Tiezhai complex in Linqu county of Western Shandong and their geological significance," *Geoscience*, vol. 34, no. 3, pp. 418–430, 2020.

[21] J. Deng, C. M. Wang, L. Bagas, M. Santosh, and E. Y. Yao, "Crustal architecture and Metallogenesis in the South-Eastern North China Craton," *Earth-Science Reviews*, vol. 182, July, pp. 251–272, 2018.

[22] G. Zhao, M. Sun, S. A. Wilde, and L. Sanzhong, "Late Archean to Paleoproterozoic evolution of the North China Craton: Key issues Revisited," *Precambrian Research*, vol. 136, no. 2, pp. 177–202, 2005.

[23] Y. F. Zheng, Z. Xu, Z. F. Zhao, and L. Q. Dai, "Mesozoic Mafic Magmatism in North China: Implications for thinning and destruction of Cratonic Lithosphere," *Science China Earth Sciences*, vol. 61, no. 4, pp. 353–385, 2018.

[24] Y. Wan, D. Liu, S. Wang, et al., " 2.7 Ga juvenile crust formation in the North China Craton (Taishan-Xintai area, Western Shandong province): Further evidence of an understated event from U-PB dating and HF isotopic composition of Zircon," *Precambrian Research*, vol. 186, nos. 1–4, pp. 169–180, 2011.

[25] C. M. Wang, Y. J. Lu, X. Y. He, Q. H. Wang, and J. Zhang, "The Paleoproterozoic Diorite Dykes in the Southern margin of the North China Craton: Insight into rift-related Magmatism," *Precambrian Research*, vol. 277, May, pp. 26–46, 2016.

[26] C. M. Wang, L. Bagas, J. Deng, and M. M. Dong, "Crustal architecture and its controls on Mineralisation in the North China Craton," *Ore Geology Reviews*, vol. 98, July, pp. 109–125, 2018.

[27] M. G. Zhai and M. Santosh, "The early Precambrian Odyssey of the North China Craton: Asynoptic overview," *Gondwana Research*, vol. 20, no. 1, pp. 6–25, 2011.

[28] M. G. Zhai, "Tectonic evolution of the North China Craton," *Journal of Geomechanics*, vol. 25, no. 5, pp. 722–745, 2019.

[29] S. Liu, C. Feng, M. Santosh, et al., "Integrated elemental and SR-nd-PB-HF isotopic studies of Mesozoic Mafic Dykes from the Eastern North China Craton: Implications for the dramatic transformation of Lithospheric Mantle," *Journal of Geodynamics*, vol. 114, February, pp. 19–40, 2018.

[30] L. Gao, S. W. Liu, B. Zhang, G. Z. Sun, Y. L. Hu, and R. R. Guo, "A ca. 2.8Ga plume-induced Intraoceanic arc system in the Eastern North China Craton," *Tectonics*, vol. 38, no. 5, pp. 1694–1717, 2019.

[31] Lei Gao, S. Liu, Y. Hu, G. Sun, R. Guo, and H. Bao, "Late Neoarchean Geodynamic evolution: Evidence from the Metavolcanic rocks of the Western Shandong Terrane, North China Craton," *Gondwana Research*, vol. 80, April, pp. 303–320, 2020.

[32] F. Y. Wu, Y. G. Xu, R. X. Zhu, and G. W. Zhang, "Thinning and destruction of the Cratonic Lithosphere: A global perspective," *Science China Earth Sciences*, vol. 12, no. 57, pp. 1674–7313, 2014.

[33] S. H. Zhang, Y. Zhao, G. A. Davis, H. Ye, and F. Wu, "Temporal and spatial variations of Mesozoic Magmatism and deformation in the North China Craton: Implications for Lithospheric thinning and Decratonization," *Earth-Science Reviews*, vol. 131, April, pp. 49–87, 2014.

[34] L. Ma, S. Y. Jiang, A. W. Hofmann, Y. G. Xu, B. Z. Dai, and M. L. Hou, "Rapid Lithospheric thinning of the North China Craton: New evidence from Cretaceous Mafic Dikes in the Jiaodong peninsula," *Chemical Geology*, vol. 432, August, pp. 1–15, 2016.

[35] J. G. Liu, R. H. Cai, D. G. Pearson, and J. M. Scott, "Thinning and destruction of the Lithospheric Mantle root beneath the North China Craton: A review," *Earth-Science Reviews*, vol. 196, September, p. 102873, 2019.

[36] W. Xu, J. M. Hergt, S. Gao, F. Pei, W. Wang, and D. Yang, "Interaction of Adakitic melt-Peridotite: Implications for the high-mg signature of Mesozoic Adakitic rocks in the Eastern North China Craton," *Earth and Planetary Science Letters*, vol. 265, nos. 1–2, pp. 123–137, 2008.

[37] L. Q. Dai, Y. F. Zheng, and Z. F. Zhao, "Termination time of peak Decratonization in North China: Geochemical evidence from Mafic igneous rocks," *Lithos*, vols. 240–243, January, pp. 327–336, 2016.

[38] S. Zou, D. Xu, T. Deng, et al., "Geochemical variations of the late Mesozoic Granitoids in the Southern margin of North China Craton: A possible link to the Tectonic transformation from compression to extension," *Gondwana Research*, vol. 75, November, pp. 118–133, 2019.

[39] K. Shi, C. Wang, M. Santosh, B. Du, L. Yang, and Q. Chen, "New insights into Neoarchean-Paleoproterozoic Crustal evolution in the North China Craton: Evidence from Zircon U-PB Geochronology, LU-HF Isotopes and geochemistry of Ttgs and Greenstones from the Luxi Terrane," *Precambrian Research*, vol. 327, July, pp. 232–254, 2019.

[40] K. X. Shi, C. M. Wang, L. Bagas, B. Du, L. F. Yang, and Q. Chen, "Genesis of the Hanwang Fe deposit in Neoarchean granite-Greenstone succession of the Eastern North China Craton," *Ore Geology Reviews*, vol. 105, February, pp. 387–403, 2019.

[41] L. Gao, S. Liu, G. Sun, et al., "Neoarchean crust-Mantle interactions in the Yishui Terrane, South-Eastern margin of the North China Craton: Constraints from geochemistry and Zircon U-PB-HF Isotopes of Metavolcanic rocks and high-K Granitoids," *Gondwana Research*, vol. 65, January, pp. 97–124, 2019.

[42] G. Zhu, D. Z. Jiang, B. L. Zhang, and Y. Chen, "Destruction of the Eastern North China Craton in a Backarc setting: Evidence from Crustal deformation Kinematics," *Gondwana Research*, vol. 22, no. 1, pp. 86–103, 2012.

[43] W. Wang, M. Zhai, S. Wang, et al., "Crustal Reworking in the North China Craton at ~2.5 Ga: Evidence from Zircon U-PB age, HF Isotope and whole rock geochemistry of the Felsic volcano-sedimentary rocks from the Western Shandong province," *Geological Journal*, vol. 48, no. 5, pp. 406–428, 2013. http://doi.wiley.com/10.1002/gj.v48.5.

[44] Y. L. Hu, S. W. Liu, G. Z. Sun, and L. Gao, "Petrogenesis of the Neoarchean Granitoids and Crustal oxidation States in the Western Shandong province, North China Craton," *Precambrian Research*, vol. 334, 2019.

[45] C. H. Yang, W. L. Xu, D. B. Yang, C. C. Liu, X. M. Liu, and Z. C. Hu, "Petrogenesis of the Mesozoic high-mg Diorites in West Shandong: Evidence from chronology and Petro-geochemistry," *Earth Science Journal of China University of Geosciences*, vol. 1, no. 31, pp. 81–92, 2006.

[46] T.-G. Lan, H.-R. Fan, F.-F. Hu, A. G. Tomkins, K.-F. Yang, and Y. Liu, "Multiple crust-Mantle interactions for the destruction of the North China Craton: Geochemical and SR-nd-PB-HF isotopic evidence from the Longbaoshan alkaline complex," *Lithos*, vol. 122, nos. 1–2, pp. 87–106, 2011.

[47] T.-G. Lan, H.-R. Fan, M. Santosh, et al., "Early Jurassic high-K Calc-alkaline and Shoshonitic rocks from the Tongshi intrusive complex, Eastern North China Craton: Implication for crust-Mantle interaction and post-Collisional Magmatism," *Lithos*, vols. 140–141, May, pp. 183–199, 2012.

[48] D. B. Yang, W. L. Xu, F. P. Pei, C. H. Yang, and Q. H. Wang, "Spatial extent of the influence of the deeply Subducted South China block on the southeastern North China block: Constraints from SR-nd-PB Isotopes in Mesozoic Mafic igneous rocks," *Lithos*, vols. 136–139, April, pp. 246–260, 2012.

[49] Y. Wang, H. R. Fan, and F. F. H. and, "Zircon U-PB ages and geochemistry of elements and Isotopes of the Diorite from Tongjing, Yinan, Western Shandong province," *Acta Petrologica et. Mineralogica (In Chinese)*, vol. 30, no. 4, pp. 553–566, 2011.

[50] Y. L. Wang, *Petrogenesis of Mesozoic High-Mg Diorites from Tietonggou in West Shandong, China*, Institute of Geology and Geophysics, CAS (In Chinese), 2011.

[51] X. L. Huang, J. W. Zhong, and Y. G. Xu, "Two tales of Thecontinental Lithospheric Mantle prior to the destruction ofthe North China Craton: Insights from Geochemical Comparisonof the early Cretaceous Mafic intrusions at western Shandong, East China," *Geochimica et Cosmochimica Acta*, vol. 96, November, pp. 193–214, 2012.

[52] J. W. Zhong and X. L. Huang, "Spatial variation of Zircon HF Isotopes for the early Cretaceous Mafic intrusions in Western Shandong and its genesis," in *Geotectonica et Metallogenia (in Chinese)*, 36:pp. 572–580, 2012.

[53] Y. W. Liang, Y. Lai, H. Hu, and F. Zhang, "Zircon U-PB ages and Geochemical characteristics study of Syenite from Weishan REE deposit, Western Shandong," in *Acta Scientiarum Naturalium Universitatis Pekinensis (In Chinese)*. Vol. 53, 2017.

[54] C. H. Yang, W. L. Xu, D. B. Yang, W. Wang, W. D. Wang, and J. M. Liu, "Genesis of the Shangyu Gabbro Diorite in Luxi Terrane: Evidence from chronology and geochemistry," *Scientia Sinica (Terrae) (in Chinese)*, vol. 38, no. 1, pp. 44–55, 2008.

[55] Z. Xu, Z. F. Zhao, and Y. F. Zheng, "Slab-Mantle interaction for thinning of Cratonic Lithospheric Mantle in North China: Geochemical evidence from Cenozoic Continental Basalts in central Shandong," *Lithos*, vols. 146–147, August, pp. 202–217, 2012.

[56] L. D. Yu, "Geological and Geochemical characteristics and Geodynamic settings of the Tiezhai complex in Linqu, Western Shandong," , [Master Thesis], China University of Geosciences (Beijing), 2018.

[57] P. Guo, M. Santosh, S. R. Li, and Q. Li, "Crustal evolution in the central part of Eastern NCC: Zircon U-PB ages from multiple Magmatic pulses in the Luxi area and implications for gold mineralization," *Ore Geology Reviews*, vol. 60, July, pp. 126–145, 2014.

[58] R. S. Zhang and Y. J. Gan, "Basic characteristics of Jinxingtou complex in Yiyuan County and the relation with gold mineralization," *Geology of Shandong Province (in Chinese)*, vol. 14, no. 4, pp. 4–15, 2001.

[59] K. R. Ludwig, *A Geochronological Toolkit for Microsoft Excel*, Berkeley Geochronology Center, California, 2003.

[60] A. Bouvier, J. D. Vervoort, and P. J. Patchett, "The LU-HF and SM-nd isotopic composition of CHUR: constraints from Unequilibrated Chondrites and implications for the bulk composition of terrestrial planets," *Earth and Planetary Science Letters*, vol. 273, nos. 1–2, pp. 48–57, 2008.

[61] W. L. Griffin, N. J. Pearson, E. Belousova, et al., "The HF Isotope composition of Cratonic Mantle: LAM-MC-ICPMS analysis of Zircon Megacrysts in Kimberlites," *Geochimica et Cosmochimica Acta*, vol. 64, no. 1, pp. 133–147, 2000.

[62] Y. S. Liu, S. Gao, Z. C. Hu, C. G. Gao, K. Q. Zong, and D. B. Wang, "Continental and Oceanic crust recycling-induced melt-Peridotite interactions in the Trans-North China Orogen: U-PB dating, HF Isotopes and trace elements in Zircon from Mantle Xenoliths," *Journal of Petrology*, vol. 51, nos. 1–2, pp. 537–571, 2010.

[63] J. D. Vervoort, P. J. Pachelt, G. E. Gehrels, and A. P. Nutman, "Constraints on early Earth differentiation from hafnium and neodymium isotopes," Nature, vol. 379, pp. 624–627, 1996.

[64] S. -S. Sun and W. F. McDonough, "Chemical and isotopic SYSTEMATICS of Oceanic Basalts: Implications for Mantle composition and processes," *Geological Society, London, Special Publications*, vol. 42, no. 1, pp. 313–345, 1989.

[65] Y. L. Hu, S. W. Liu, Z. L. Jin, Q. H. Xie, B. B. Wen, and Z. X. Li, "Petrogenesis of Hornblendite Enclaves in Jinling Magmatic Complex of Intrusions from the Western Shandong Province," Acta Scientiarum Naturalium Universitatis Pekinensis (In Chinese), vol. 54, no.2, pp. 385–397, 2018.

[66] T. Donaire, E. Pascual, C. Pin, and J. L. Duthou, "Microgranular enclaves as evidence of rapid cooling in granitoid rocks: The case of the Los Pedroches granodiorite, Iberian Massif, Spain," Contributions to Mineralogy and Petrology, vol. 149, pp. 247–265, 2005.

[67] Y. G. Xu, X.-L. Huang, J.-L. Ma, et al., "Crust-Mantle interaction during the Tectono-thermal reactivation of the North China Craton: constraints from SHRIMP Zircon U-PB chronology and geochemistry of Mesozoic Plutons from Western Shandong, " *Contributions to Mineralogy and Petrology*, vol. 147, no. 6, pp. 750–767, 2004.

[68] Y. Zhu, S. Lai, J. Qin, et al., "Magma mixing for the genesis of Neoproterozoic Mopanshan Granitoids in the Western Yangtze block, South China," *Journal of Asian Earth Sciences*, vol. 231, June, p. 105227, 2022.

[69] M. J. Farner, C. T. A. Lee, and K. D. Putirka, "Mafic-Felsic Magma mixing limited by reactive process: A case study of Biotite-rich Rinds on Mafic enclaves," *Earth and Planetary Science Letters*, vol. 393, May, pp. 49–59, 2014.

[70] J. D. Clemens and G. Stevens, "What controls chemical variation in Granitic Magmas?," *Lithos*, vols. 134–135, March, pp. 317–329, 2012.

[71] X.-H. Ma, C.-J. Chen, J.-X. Zhao, S.-L. Qiao, and Z.-H. Zhou, "Late Permian intermediate and Felsic intrusions in the Eastern central Asian Orogenic belt: Final-stage Magmatic record of paleo-Asian Oceanic Subduction," *Lithos*, vols. 326–327, February, pp. 265–278, 2019.

[72] S. R. Taylor and S. M. McLennan, *The Continental Crust: Its Composition and Evolution*, Blackwell, Oxford, 1985.

[73] R. P. Rapp and E. B. Watson, "Dehydration melting of Metabasalt at 8–32 Kbar: Implications for Continental growth and crust–Mantle recycling," *Journal of Petrology*, vol. 36, no. 4, pp. 891–931, 1995.

[74] C. R. Stern and R. Kilian, "Role of the Subducted slab, Mantle wedge, and Continental crust in the generation of Adakites from the Austral volcanic zone," *Contributions to Mineralogy and Petrology*, vol. 123, no. 3, pp. 263–281, 1996.

[75] M. P. Atherton and N. Petford, "Generation of sodium-rich Magmas from newly Underplated Basaltic crust," *Nature*, vol. 362, no. 6416, pp. 144–146, 1993.

[76] A. J. Brackman and J. J. Schwartz, "The formation of high-SR/Y Plutons in Cordilleran-arc crust by crystal accumulation and melt loss," *Geosphere*, vol. 18, pp. 370–393, 2022.

[77] R. F. Weinberg and P. Hasalová, "Water-Fluxed melting of the Continental crust: A review," *Lithos*, vols. 212–215, January, pp. 158–188, 2015.

[78] F. Holtz, W. Johannes, N. Tamic, and H. Behrens, "Maximum and minimum water contents of Granitic melts generated in the crust: A reevaluation and implications," *Lithos*, vol. 56, no. 1, pp. 1–14, 2001.

[79] F. Holtz, J. Roux, S. Ohlhorst, H. Behrens, and F. Schulze, "The effects of silica and water on the viscosity of hydrous Quartzofeldspathic melts," *American Mineralogist*, vol. 84, nos. 1–2, pp. 27–36, 1999.

[80] M. B. Wolf and P. J. Wyllie, "Dehydration-melting of Amphibolite at 10 Kbar: The effects of temperature and time," *Contributions to Mineralogy and Petrology*, vol. 115, no. 4, pp. 369–383, 1994.

[81] R. P. Rapp, N. Shimizu, M. D. Norman, and G. S. Applegate, "Reaction between slab-derived melts and Peridotite in the Mantle wedge: Experimental constraints at 3.8 Gpa," *Chemical Geology*, vol. 160, no. 4, pp. 335–356, 1999.

[82] F. Xue, M. Santosh, T. Tsunogae, and F. Yang, "Geochemical and isotopic imprints of early Cretaceous Mafic and Felsic Dyke suites track Lithosphere-Asthenosphere interaction and Craton destruction in the North China Craton," *Lithos*, vols. 326–327, February, pp. 174–199, 2019.

[83] C. R. Diwu, Y. Sun, H. L. Yuan, H. L. Wang, X. P. Zhong, and X. M. Liu, "Detrital Zircon U-PB Geochronology and HF isotopic composition of Songshan Quartzite from Southern Dengfeng area and its geological significance," *Science (New York, N.Y.)*, vol. 53, no. 16, pp. 1923–1934, 2008.

[84] F. Liu, J. H. Guo, X. P. Lu, and C. R. Diwu, "Crustal growth at -2.5 Ga in the North China Craton: evidence from whole-rock Nd and zircon Hf isotopes in the Huai'an gneiss terrane," Chinese Science Bulletin, vol. 54, no.24, pp. 4704–4713, 2009.

[85] L. Wan, Z. X. Zeng, T. Kusky, et al., "Geochemistry of middle-late Mesozoic mafic intrusions in the eastern North China Craton: New insights on lithospheric thinning and decratonization," Gondwana Research, vol. 73, pp. 153–174, 2019.

[86] E. Slaby and H. Martin, "Mafic and Felsic Magma interaction in Granites: The Hercynian Karkonoszepluton (Sudetes, Bohemian Massif)," *Journal of Petrology*, vol. 49, no. 2, pp. 353–391, 2008.

[87] Z. Zhao, S. Liang, M. Santosh, and J. Wei, "Lithospheric extension associated with slab rollback: Insights from early Cretaceous Magmatism in the Southern segment of tan-LU fault zone, central-Eastern China," *Lithos*, vols. 362–363, June, p. 105487, 2020.

[88] W.-L. Ling, R.-C. Duan, X.-J. Xie, et al., "Contrasting geochemistry of the Cretaceous volcanic suites in Shandong province and its implications for the Mesozoic lower crust Delamination in the Eastern North China Craton," *Lithos*, vol. 113, nos. 3–4, pp. 640–658, 2009.

[89] T. M. Kusky, B. F. Windley, L. Wang, Z. Wang, X. Li, and P. Zhu, "Flat slab Subduction, trench suction, and Craton destruction: Comparison of the North China, Wyoming, and Brazilian Cratons," *Tectonophysics*, vol. 630, September, pp. 208–221, 2014.

[90] Q.-K. Xia, J. Liu, S.-C. Liu, I. Kovács, M. Feng, and L. Dang, "High water content in Mesozoic primitive Basalts of the North China Craton and implications on the destruction of Cratonic Mantle Lithosphere," *Earth and Planetary Science Letters*, vol. 361, January, pp. 85–97, 2013.

[91] X. Geng, S. F. Foley, Y. Liu, Z. Wang, Z. Hu, and L. Zhou, "Thermal-chemical conditions of the North China Mesozoic Lithospheric Mantle and implication for the Lithospheric thinning of Cratons," *Earth and Planetary Science Letters*, vol. 516, no. 15, pp. 1–11, 2019.

[92] J. Xu and Z. Li, "Middle–late Mesozoic sedimentary Provenances of the Luxi and Jiaolai areas: Implications for Tectonic evolution of the North China block," *Journal of Asian Earth Sciences*, vol. 111, November, pp. 284–301, 2015.

[93] J. Zhang, S. Z. Li, X. Y. Li, et al, "Yanshanian deformation of the Luxi area: Tectonic response to the paleo-Pacific plate Subduction," *Earth Science Frontiers (in Chinese)*, vol. 24, no. 4, pp. 226–238, 2017.

[94] C. H. Yang, W. L. Xu, D. B. Yang, C. Liu, X. Liu, and Z. Hu, "Chronology of the Jinan Gabbro in Western Shandong: Evidence from LA-ICP-MS Zircon U-PB dating," *Acta Geoscientica Sinca*, vol. 26, no. 4, pp. 321–325, 2005.

[95] A. L. Streckeisen and R. W. Maitre, "A chemical approximation to the modal QAPF classification of the igneous rocks," *Neues Jahrb Mineral., Abh*, vol. 136, 1979.

[96] K. C. Condie, "Chemical composition and evolution of the upper Continental crust: Contrasting results from surface samples and Shales," *Chemical Geology*, vol. 104, nos. 1–4, pp. 1–37, 1993.

[97] M. J. L. Bas, R. W. L. Maitre, A. Streckeisen, B. Zanettin, and IUGS Subcommission on the Systematics of Igneous Rocks, "A chemical classification of volcanic rocks based on the total alkali-silica diagram," *Journal of Petrology*, vol. 27, no. 3, pp. 745–750, 1986.

[98] B. Jahn and Z. Zhang, "Archean Granulite Gneisses from Eastern Hebei province, China: Rare earth geochemistry and Tectonic implications," *Contributions to Mineralogy and Petrology*, vol. 85, no. 3, pp. 224–243, 1984.

[99] A. Peccerillo and S. R. Taylor, "Geochemistry of Eocene Calc-alkaline volcanic rocks from the Kastamonu area, northern Turkey," *Contributions to Mineralogy and Petrology*, vol. 58, no. 1, pp. 63–81, 1976.

[100] W. F. McDonough and S. -S. Sun, "The composition of the earth," *Chemical Geology*, vol. 120, nos. 3–4, pp. 223–253, 1995.

[101] Q. Wang, D. A. Wyman, J. Xu, et al., "Early Cretaceous Adakitic Granites in the northern Dabie complex, central China: Implications for partial melting and Delamination of thickened lower crust, " *Geochimica et Cosmochimica Acta*, vol. 71, no. 10, pp. 2609–2636, 2007.

[102] D. J. H. C. Liu and Y. L. Li, "Large-scale early Cretaceous lower-crust melting derived Adakitic rocks in NE China:

Implications for CONVERGENT Bidirectional Subduction and slab rollback," *International Geology Review*, vol. 62, pp. 2324–2343, 2010.

[103] H. Martin, "Effect of steeper Archean geothermal gradient on geochemistry of Subduction-zone Magmas," *Geology*, vol. 14, no. 9, 1986.

[104] J. M. Ferry and E. B. Watson, "New thermodynamic models and revised calibrations for the TI-in-Zircon and Zr-in-Rutile thermometers," *Contributions to Mineralogy and Petrology*, vol. 154, no. 4, pp. 429–437, 2007.

[105] D. Trail, E. Bruce Watson, and N. D. Tailby, "Ce and EU anomalies in Zircon as proxies for the oxidation state of Magmas," *Geochimica et Cosmochimica Acta*, vol. 97, November, pp. 70–87, 2012.

[106] J. Myers and H. P. Eugster, "The system Fe-SI-O: Oxygen buffer calibrations to 1500K," *Contributions to Mineralogy and Petrology*, vol. 82, no. 1, pp. 75–90, 1983.